ALMA MATER STUDIORUM – UNIVERSITA' DI BOLOGNA

DEPARTMENT OF ELECTRICAL, ELECTRONIC AND INFORMATION ENGINEERING "GUGLIELMO MARCONI"

MASTER'S DEGREE IN TELECOMMUNICATIONS ENGINEERING

MASTER THESIS

in

Electromagnetic Propagation for Wireless Systems

ANALYSIS OF ROOF-TO-STREET PROPAGATION FOR FIXED BROADBAND WIRELESS ACCESS

CANDIDATE:
DEMMI GERARDO NAHUEL

SUPERVISOR:
Prof. Ing. FRANCO FUSCHINI

CO. SUPERVISOR:
Prof. Ing. MARINA BARBIROLI

Ing. ALESSANDRO VARINI

Academic Year 2020/2021

Index

Introduction

Fixed Wireless Access (FWA) is an alternative solution to fiber that leverages mobile wireless technology to deliver internet connectivity to the final user in an affordable way. FWA is not new, indeed there are already commercial solutions based on 4G/LTE or WiMAX, but it has not gained the expected attention by the market, because the achievements were not satisfactory. Now, with the advent of 5G New Radio (5G NR), its capabilities can be fully exploited bringing several advantages. For instance, it enables mobile operators to offer subscribers fiber-like services with higher throughput and lower latency accelerating also the 5G network rollout and increasing the market that, according to predictions, is expected to grow about 84% until 2025, surpassing USD 40 billion worldwide, as reported in [1].

With respect to the Fiber-To-The-Home (FTTH) and any other wired solutions, no complex engineering works at customer end are needed, just the provision of the Customer Provided Equipment (CPEs), which can be self-installed by the subscriber or by an expert technician. When dimensioning a FWA network, two meaningful factors must be considered: the received power at CPE side and the estimation of the signal attenuation. In order to identify the best place where to locate the equipment, a detailed analysis is needed to investigate how the signal propagates and interacts with the radio environment, thus propagation models help us to achieve this important goal. Nowadays, several models of different kind and complexity have been studied and developed with the common assumption that the user equipment is at street level. Unfortunately, this restriction is not suitable for FWA commercial applications, since the receiving antenna should be placed higher than ground level for a good reception for both indoor and outdoor places, therefore it is necessary to tune these models for a more flexible analysis.

The present work has statistically assessed the roof-to-user correction factor, here called *floor gain factor*, to take into account the actual placement of Customer Premise Equipment (CPE) with respect to the ground level. In particular, we provide the proper adjustment to propagation models at different heights from the ground, in order to have the right prediction of signal attenuation, in the 3.6 GHz frequency band. In this study, hundreds of measured points have been stored, where each of them represents a value of received signal intensity in dBm at a specific height and location, collected in different and quite far towns in Italy, involving heterogeneous type of buildings for

better results. Afterwards, for each point, we computed the difference with the received power at street level and, finally, calculated the statistical mean and standard deviation.
A physical-statistical propagation model has been developed based on the geometrical theory of propagation in the Roof-To-Street (RTS) environment, i.e., considering only the last part of the path that includes the buildings right before and after the receiver.
For simplicity, we assumed the received signal is given by different contributions as direct ray, one and multiple reflections, diffracted ray and diffracted-reflected ray. The aim is to validate empirical data and to support the analysis, offering the opportunity to examine each single ray and get more detailed information on how radio propagation mechanisms work in the roof-to-street (RTS) case.
The statistical study conducted on simulated and empirical results agree and both show the same trend, according to which the greater the height, evaluated with respect to the ground, the higher the floor gain factor. Moreover, we realized that diffraction and diffraction-reflection are the main contributions to the total received below the roof. When it is crossed, then the direct ray becomes the dominant component.
The present work starts from a general introduction to 5G technology, describing the three macro-areas where major innovations will be introduced and moving to a general description of 5G FWA systems. Next, in Chapter 2, we describe the geometrical theory of propagation, the basis of the developed mathematical model for simulation. Then we explain the measurement campaign conducted, describing the instrumentation used and the selection criteria for measurement sites. Finally, in chapters 4 and 5, the propagation model is presented, both empirical and simulated data are analysed and also compared.

Chapter 1

Fixed Wireless Access for wireless mobile broadband access

1.1 *Brief introduction to 5G*

The era of wireless communications emerged few decades ago and has helped people to exchange information as never done before in the human history. They have become ubiquitous and so essential in our daily life that we might be in trouble when absent. This was possible thanks to the extraordinary improvement in telecommunication's world restless promoted year by year. From the early development stage up to the on-going deployment of the Long – Term Evolution (LTE, also known as 4G) the main purpose of wireless networks was connecting people, that is the development of cellular standards with faster data-rates and lower latency. However, after its launch, telco companies became aware of a new kind of user with totally different requirements, i.e., the electronic devices of the Internet of Things that, despite such technology was not able to fully accomplish their constraints, undergone a great expansion. Because of this, as time goes by, cellular service providers faced continuously increasing demand for larger network capacity, higher energy efficiency, higher mobility, higher reliability and lower latency required by new wireless applications, along with the ability to provide services to users with totally different needs over the same network infrastructure.
To address the above challenges, we need a dramatic change in the design of cellular architecture and the 5G New Radio (5G NR) is the key technology to accomplish this goal. The innovations it will bring have been defined in three macro categories: Enhanced Mobile Broadband (eMBB), Ultra-Reliable Low-Latency Communications (URRLC) and Massive IoT, shortly explained here.

1.1.1 *Enhanced Mobile Broadband*

It reflects an enhancement of the mobile broadband use cases supported by the LTE standard and denotes an improvement in spectral efficiency and available bandwidth

along with the use of new bands in the so-called millimetre waves to support even higher data rates and more traffic demands. As stated by the 3GPP, user experienced data rates vary from 1 Gbps downlink and 500 Mpbs uplink for indoor environments to 50 Mbps downlink and 25 Mbps uplink for rural macro environments, whereas capacity targets can be as high as 15 Tbps/km2 with 250 000 users/km2 for indoor spots.

FWA is an eMBB specific use-case that leverages 5G beamforming and massive MIMO over higher spectrum-bands to deliver broadband connectivity across previously unreachable areas delivering good quality services. As 5G FWA becomes widely available, it can offer coverage around the world making the broadband connection available everywhere.

1.1.2 *Ultra-Reliable Low-Latency Communications*

It is related to the idea of using wireless communications at a large scale to support critical tasks by establishing resilient connections with very low latency budget providing support to real-time applications. For instance, it is suitable for vehicle-to-vehicle (V2V) communication where requirements are reliability > 99.999 % and latency < 1 millisecond. Other important examples are factory automation, motion control and process automation.

Among all the use-cases, this is one of the most challenging because latency and reliability are often in contrast. Indeed, if the former increases, the latter increases as well (e.g., higher latency budget allows more retransmissions to take place). On the other hand, higher reliability means lower throughput, because it requires more powerful coding schemes including more redundant bits, hence less throughput.

1.1.3 *5G MTC*

Its main focus is on transmitting low data volumes occasionally to and from very large numbers of devices that require wide area coverage and long battery life over a network infrastructure that is expected to be energy-efficient, thus being perfect for IoT. It has two aspects:

- mMTC: means massive machine-type communication and is characterized by a large number of connected devices typically transmitting a relatively low volume of non-delay-sensitive data.

- uMTC: or Ultra-reliable Machine Type Communication and focuses on reliability and low latency.

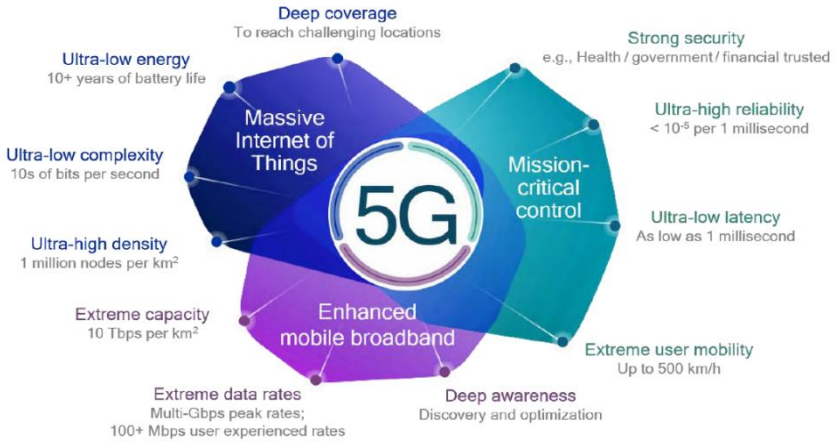

Fig. 1.1: The three 5G macro areas.

1.2 *5G Fixed Wireless Access*

As stated in the previous paragraphs, 5G FWA is expected to be a very efficient method to economically support broadband access to homes and small and medium-sized enterprises, in sub-urban and rural scenarios or, in other words, as long as the number of households (HH) in a given area is not too high. According to A. Gravey et al. [2], fiber technology is profitable and economically reasonable when user density is high, around 5000 HH/km^2, to justify the operational expenditure and the more substantial capital expenditure which includes civil engineering costs, e.g., digging and trenching to lay new ducts for fiber and optical network unit installation for each subcriber performed by a technician. On the other hand, urban areas are less challenging and more suitable for such kind of work than rural and suburban scenarios, which might become a market failure area as not attractive. Therefore, we can think of fixed wireless access as the bridge between MBB and fixed broadband, especially in the last mile towards the end user's building, lowering the average per connection costs. This technology has other benefits and weaknesses, listed below.

Benefits:

- Quick Provisioning: with FWA, the service activation time is reduced to a minimum, since once equipped with the appropriate modem (indoor solution), it is necessary to insert the operator's SIM card to start surfing immediately,

unlike the fiber that usually takes weeks from service requests to service activation.

- Mobility: it allows to move the connection in a different place from your home simply by placing the router (with SIM inserted) in the desired place, because the system relies on the cellular network. Same, in case the outdoor solution is adopted.

- Flexible contracts: rechargeable as they are SIM based, like a cell phone, thus great for a backup connection.

Weaknesses:

- Cell traffic load: base stations have to deal with much more users within the same cell and this might lead to saturation during peak hours.

- Atmospheric agents as rain or snow could affect signal propagation due to refraction\reflection on water drops or snow crystals, causing higher signal attenuation. This becomes more and more prominent phenomenon as frequency increases.

- In urban environment, it may happen that the CPE cannot be in line of sight with the base station, therefore propagation impairments may arise making the positioning critical

An important aspect is that 5G FWA operates both in licensed and unlicensed bands. The former includes 3.4-3.6 GHz auctioned in 2008, 3.6-3.8 GHz and the relatively new mmwave frequencies 26.5-27.5 GHz, suitable for massive MIMO. The latter consists of the 5.4 GHz band only.
In the FWA network architecture, there is a radio base station (RBS) wirelessly connected to a *fixed wireless access user equipment*, consisting of a receiving antenna, in turn linked to a Customer Premise Equipment (CPE), which delivers connectivity in user's home, as depicted in the following picture.

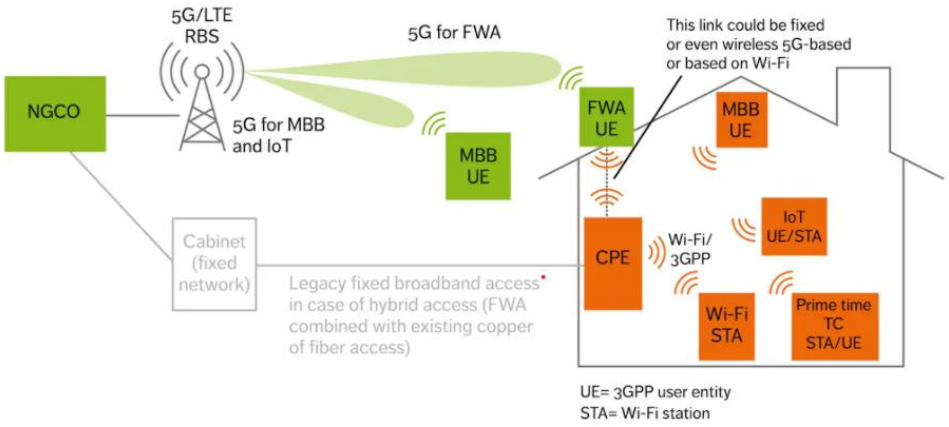

Fig 1.2: FWA system architecture

Moreover, coverage and overall performance largely depend on the propagation environment or terrain the system operates in and on the signal frequency. As a consequence, a hybrid antenna's placement solution is necessary, where users closer to the RBS have outdoor wall-mounted or indoor equipment and those who are further use rooftop antennas. However, due to rapid installation or other reasons, not always the CPE can be mounted on the roof top it may happen that sometimes it is installed vertical wall next to the user's household, making the propagation more vulnerable. In the outdoor case, with high-gain CPE, a coverage radius of 30 km or greater can be envisaged, meeting the needs of both suburban and rural regions.

As stated in the white paper published by Huawei [4], the 5G FWA is the last stage of a three-step system evolution. The first phase is called *fast win*, characterised by the reuse of existing MBB RAN infrastructure to maximize network resources and quickly offer household network connections where absent. Subsequently, during phase two named *fiber-like experience*, the number of services and subscribers grow, TDD dedicated network are built and more resources are allocated. Finally, as mentioned before, 5G FWA is introduced.

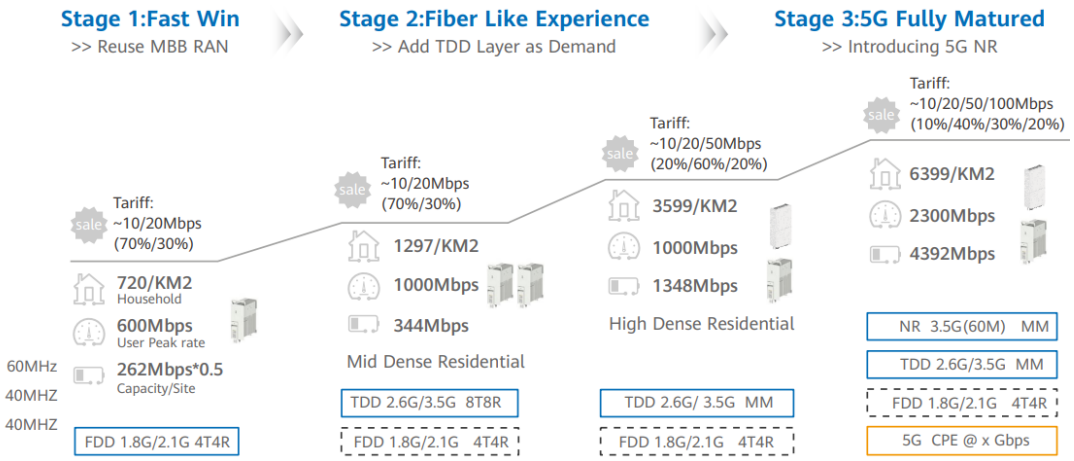

Fig. 1.3: FWA system evolution

1.3 *Digital divide*

In previous paragraphs, I introduced some significant characteristics related to the last generation of mobile radio technology. Besides all the aforementioned aspects, the digital divide represents an issue that still affects people even though Internet continues to grow. This phenomenon refers to the worldwide social issue of the different amount of information between those who have access to internet and those who don't.
Its effects visible all around the globe and no country is exempt. In Italy, for example, has a lot of digital divide areas, from isolated spots where connectivity might be absent to towns, localized in more industrialized zones, in territories whose shape makes the connectivity hard to build, usually offering poor network performances.

According to the International Telecommunication Union (ITU) [5], over 1 billion new Internet users have been added over the last five years, yet under half the world's population, 3.7 billion, still do not have access and most of them live in least developed countries (LDCs). Considering all Internet users, 87% are in developed countries and 44% in developing countries.

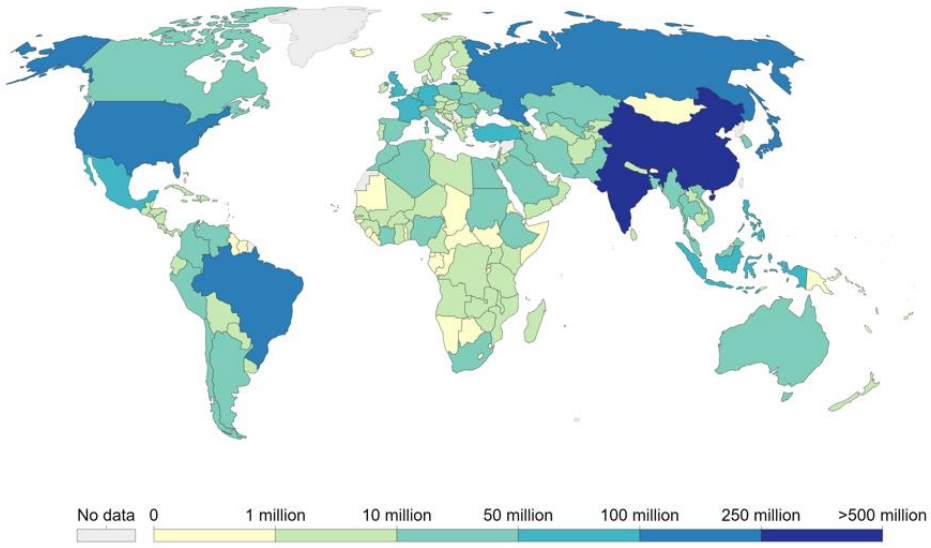

Fig. 1.4: Number of internet users by country

Generally speaking, it is a very complex phenomenon that not only concerns the access to the Web because, even if possible, further relevant aspects are involved:

- *Quality of service*: the signal strength and available services are often poor and not sufficient to guarantee basic functions as surfing the web or the access to

cloud services. For instance, in LDCs 19% of the rural population is covered only by 2G network.

- *Affordability*: is the main issue in developing countries and LDCs. It is related to inaccessibility to internet connection and digital devices like smartphones, computers and tablets, because are expensive. As a consequence, children and young people from the poorest families, rural areas and lower income states are left behind their peers in terms of digital inclusion, facing unequal exposure to poverty and unemployment.

- *Awareness*: elder people are more likely not able to access internet due to a lack in their knowledge on the topic than younger generations.

- *Gender*: globally, 42% for men are not online compared to 52% of women. More evident in the Arab States, Asia-Pacific and Africa.

- *Geography*: small nations, as Taiwan for instance, are easier to connect compared to bigger countries as Brazil or Russia that are enormously more challenging because more physical infrastructure to cover all the area is needed. In addition, the terrain plays an important role, since it may not make it easy to build dense urban structure. Indeed, it is easier to bring connectivity in wide and plane areas rather than mountain spots.

By looking at the picture below, we can realize that there is a correlation between the monthly GNI per capita and the price for both mobile and fixed broadband, which is the main obstacle. In particular, developing and LDCs' values are still higher than the 2% threshold defined by ITU (red dotted segment) in line with the Broadband Commission for Sustainable Development program. Even though for some countries the mobile broadband is above the target, it is still a viable solution and the fixed wireless access, even better in combination with 5G, could be a good opportunity to improve the broadband penetration at global level, especially in developing countries, offering robust services with acceptable data rates to the user and representing a valid countermeasure to mitigate the effects of Digital Divide phenomenon.

Chapter 2

Fundamentals of Urban Propagation

Existing propagation models are not suitable for FWA applications as they do not allow a correct prediction in this case. Based on this assumption, we started a measurement campaign that aims at statistically find the correction factor that helps mobile operators to have a correct evaluation of the final signal attenuation based on the height. In addition, we decided to perform a simulation in order to better investigate how the propagation takes place. The theoretical basis behind the model found is the *geometrical theory of propagation* (GTP) that will be described in this chapter in view of the simulation explained in chapter 4.

The electromagnetic propagation in real environments, such as urban or rural, is usually very complex to analyse by analytically solving the Maxwell equations. Surely it is the best way to accurately express the electromagnetic field and all of its components in space and time. Nevertheless, this approach is usually not feasible and very complex to deal with since the multipath nature of the wireless channel, due to the presence of obstacles between transmitter and receiver, that make the propagation very complicated. Thus, it is much more convenient to introduce some approximations to simplify the problem and the description for a faster understanding by means of the geometrical theory of propagation, which is more intuitive and allows to handle hard problems more easily, setting the basis for ray-tracing algorithms. Moreover, we can analyse phenomena as refraction, reflection, diffraction and scattering by simply drawing rays, thus being particularly beneficial to investigate propagation within inhomogeneous medium. After the introduction to optical geometry, general description of propagation models is presented to finally move to those typically used for FWA systems.

2.1 *Introduction to Geometrical theory of propagation*

The geometrical theory of propagation is based on geometrical representation of electromagnetic waves in the far field region though the knowledge of rays' trajectories from transmitter to receiver. The ray, in turn, is a curved or straight spatial line

perpendicular in each point to the equiphase surface of the propagating electromagnetic field.

2.1.1 *GTP main equations*

In presence of source-less volume filled with loss-less (γ=0) mildly inhomogeneous medium, the corresponding field equation can be written as:

(2.1) $\overrightarrow{E(r)} = \overrightarrow{E_0(r)} \cdot e^{-j\beta_0\psi(\vec{r})}$ (2.2) $\overrightarrow{H(r)} = \overrightarrow{H_0(r)} \cdot e^{-j\beta_0\psi(\vec{r})}$

In the previous equations the term $\psi(\vec{r})$ is known as the *eikonal function,* according to which the set of points with $\psi(\vec{r})$ = constant define the warfront.
The expressions (2.1) and (2.2) are obtained from a generalization of the homogeneous case and can actually represent the real field if they satisfy the Maxwell's equations.
Now, for sake of simplicity, I refer to the electric field only, but same considerations still hold for the magnetic field as well. Under the assumption of frequency f → +∞ and wavelength λ → 0, we put (2.1) and (2.2) into Maxwell's equation and we get:

(2.3) $|\nabla\psi|^2 = n^2(\vec{r})$ → (2.4) $\nabla\psi(\vec{r}) = n(\vec{r})$

(2.4) $\overrightarrow{E_0}\nabla^2\psi + 2\overrightarrow{\nabla\psi}\left[\overrightarrow{E_0} \cdot \overrightarrow{\nabla \ln(n)}\right] + 2\left(\overrightarrow{\nabla\psi} \cdot \vec{\nabla}\right)\overrightarrow{E_0} = 0$

Note that, basically, the above requirement says that the smaller the wavelength is the more accurate the approximation (that's why we usually speak about optical geometry) and it is practically satisfied as long as the refraction index of propagation medium slowly varies in space with respect to λ.
The expressions (2.3) and (2.4) are the *eikonal equation* and *transport equation* respectively and denote the set of fundamental equations of geometrical theory.
If the medium's properties are known, i.e., how the refraction index $n(\vec{r})$ changes over space, we can solve the (2.3) to obtain the eikonal function in each point (x,y,z) and then trace the wavefronts and rays.
Now, we can rewrite the equation (2.3) as:

(2.5) $\hat{S} = \frac{\nabla\psi(\vec{r})}{n(\vec{r})}$

This equation characterizes a change in the perspective: instead of find the equiphase surface, we look for the local direction perpendicular to that surface. Therefore, $\hat{s}$ is the direction of the *ray*.
After some mathematical steps, we get the *differential ray equation*, that allows to investigate ray's trajectories without any preliminary knowledge of the eikonal function but knowing the $n(\vec{r})$ profile only.

$$\frac{d}{ds}\left(n\frac{d\vec{r}}{ds}\right) = \vec{\nabla}n \tag{2.6}$$

Starting from this equation, one could demonstrate that the ray always steers towards the region of space with higher refraction index.
So far the way to obtain and trace rays has been shown, now, with this information in mind , we must compute the field along it, i.e., we need to know how the field's phase and amplitude evolves over the ray.
The former, is defined by $\psi(s)$, a function of the local variable s along the ray that describes the phase shift experienced by the field because of propagation.
The latter is identified by the *spreading factor*, a term related to the distribution of the emitted energy along the wave surface of the radiated field and describes how the amplitude decreases along the ray. To better understand the concept, let us evaluate the energy distributed over a spherical surface (point source) of a field propagating in a lossless medium. As the distance increases, the radius increases as well, consequently the propagating energy is distributed over a larger and larger surface area, which, due to the principle of conservation of energy, causes the amplitude of the field to decrease. Thus, the spreading factor is always lower or equal than one, where the equality is verified only in case of plane waves. Finally, the complete expression of the field for each point along the ray is:

$$\vec{E}(s) = \vec{E}(s_0) \cdot SF \cdot e^{-j\beta_0 ns} \tag{2.7}$$

In other words, if we know the field in the reference point s_0 we can easily forecast its evolution along the ray.

2.2 *Propagation mechanisms in presence of obstacles*

The electromagnetic field usually interacts with obstacles when emitted in a terrestrial environment, . Typical interaction mechanisms are:

- Reflection/refraction
- Diffraction
- Scattering

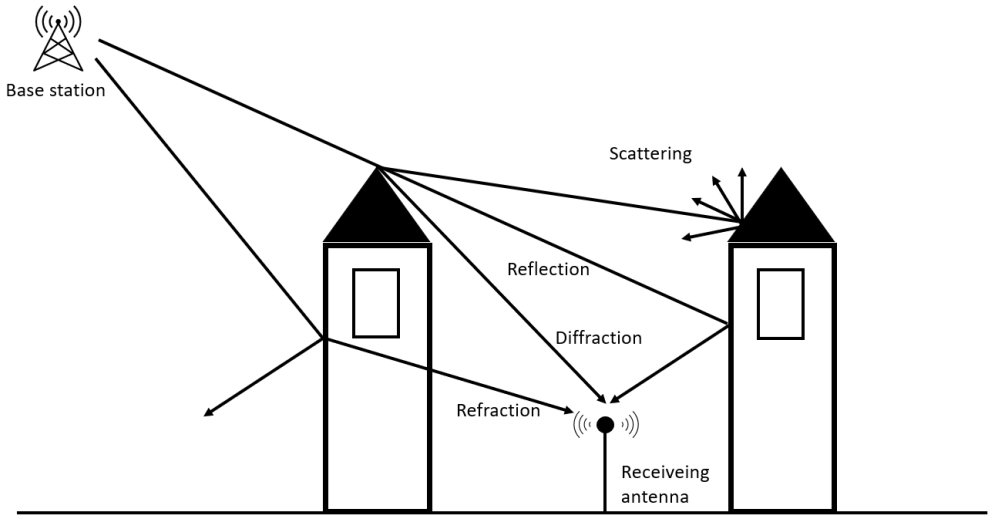

Fig 2.1: Main propagation mechanisms when obstacles are present

In some cases, these mechanisms are useful for reception in NLOS areas, without which it would be impossible. The long-range propagation over the troposphere is a good example: the troposphere refraction index is not constant in time and space. The function depends on parameters as temperature, pressure, water vapour content and altitude, in particular it exponentially decreases as the height increases. As consequence, when the wireless link distance is quite long (approximately tens of kilometres or more), rays tend to follow circular trajectories being able to reach receivers hidden by the earth's curvature, as long as link's antennas are properly steered.

In other circumstances, on the other hand, are a source of noise and distortion which can lead to undesirable problems, if not properly treated.

2.2.1 *Reflection/Refraction*

The physical phenomenon occurring when a ray impinges on the discontinuity surface interposed between two propagating media. With reference to the figure 2.1, the

reflected ray has the trajectory deflected by an angle equal to that of the incident ray with reference to the normal, as stated in Snell's law for reflection.
Refraction arises in the same way as reflection, but this time, the refracted ray propagates in the second medium with a transmission angle, defined by Snell's law for refraction.

2.2.2 *Diffraction*

The definition of diffraction is the spreading of waves as they pass through or around an obstacle. In general, diffraction of electromagnetic of waves occurs when they pass by a corner or through an opening or hole, whose size or curvature is physically the approximate size of, or even smaller than the wavelength λ. Recalling the GTP, diffraction was first described by Keller, whose law defines diffracted rays' trajectories. According to the theory, they belong to the *Keller's cone* lateral surface having vertex where the ray impinges and semi-aperture equal to the angle between the incident ray and the edge.

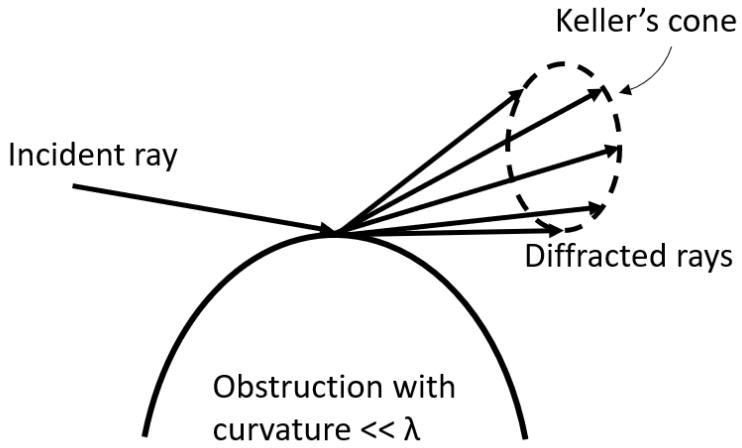

Fig. 2.2: Diffracted rays and obstruction's curvature << λ

The Uniform Theory of Diffraction (UTD) and optical geometry are the theoretical basis behind the model and are employed to calculate the field along the rays.
It starts from the simplification of obstacles over vertical plane by replacing them with an array of *knife-edges* (KE), source of diffraction depicted as a line with infinitesimal width and height equal to that of the associated obstacle, in order to estimate the excess path loss due to multiple refraction over the top of obstacles impeding the LoS in the vertical plane. Then, the first Fresnel's ellipsoid is drawn around terminals to quantify the obstruction's effects on propagation, since it has been shown that it can

dramatically worsen the reception when present even if the direct path is clear. Therefore, it is important to determine whether the propagation may approach the free-space condition, which in turn requires at least 60% clearance of such region of space to take place, according to a practical rule. If the condition is not met the excess loss is considered.

The Fresnel's parameter related to the first Fresnel ellipsoid is calculated with the following formula:

$$(2.9)\quad \nu = h \cdot \sqrt{\frac{2(a+b)}{\lambda ab}}$$

Where parameters *h*, *a* and *b* are distances evaluated as shown in the picture 2.2 below. Now, we can compute the excess path loss with Lee's simplified formulas.

$$(2.10)\quad L(\upsilon)\,(dB) = \begin{cases} -20\log(0.5 - 0.62\upsilon) & -0.8 < \upsilon < 0 \\ -20\log(0.5\exp(-0.95\upsilon)) & 0 < \upsilon < 1 \\ -20\log\left[0.4 - \sqrt{0.1184 - (0.38 - 0.1\upsilon)^2}\right] & 1 < \upsilon < 2.4 \\ -20\log(0.225/\upsilon) & \upsilon > 2.4 \end{cases}$$

Note that the excess path loss < 0 means that h < 0, then it is lower than the case when h > 0, because here the direct ray is not blocked being thus the most dominant contribution at receiver side increasing the power with respect to the other case.

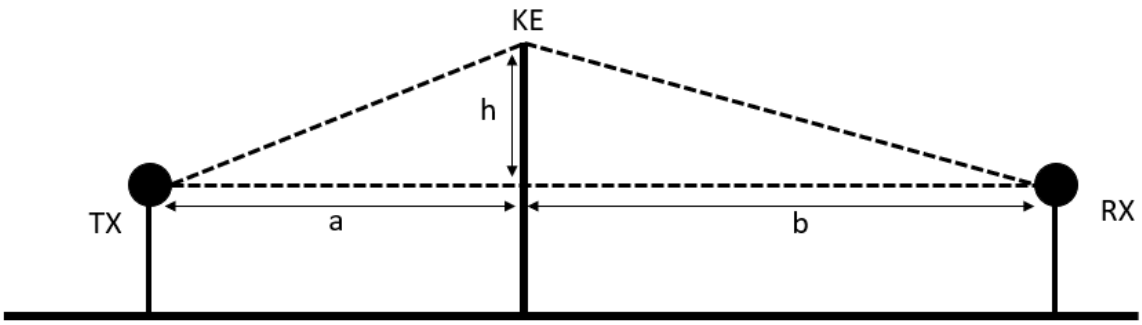

Fig. 2.3: Epstein-Peterson model's reference scheme

2.2.3 *Scattering*

Real objects are never perfectly smooth and flat with infinite extension, but rather they have a certain "roughness" degree, a measure of how much the surface is far from being ideally flat. As a consequence, when an electromagnetic wave interacts with such an obstacle, the power is in general re-irradiated in several spatial directions not limited to those of reflected, diffracted and refracted.

2.3 *Introduction to propagation models*

The 3.6-3.8 GHz has been allocated for FWA systems and is considered a good spectrum applicant and promising. Its technical characteristics make it suitable for applications in urban environment, as it represents a good compromise between coverage and capacity. It is especially useful for 5G deployment because it can provide a large amount of contiguous spectrum that will support channels with very large bandwidth, ideal for 5G deployment.

Radio spectrum is a scarce resource and must be efficiently used to deliver widespread wealth-creating services, thus research projects have to investigate the wireless channel which govern propagation and define the signal impairments in order to find accurate and valid propagation models, crucial for network planning phase and beneficial for initial deployment, feasibility studies, performance prediction and to optimally configure FWA systems, making them robust against noise and interference.

A propagation model is a procedure for the radio wave propagation prediction, characterised by a level of accuracy that measures the capability to include all the aspects related to propagation as time/frequency/angle dispersion, path loss, fading and shadowing. In addition, these models have limited validity domain, that is, a good estimation is guaranteed if and only if some requirements in terms of frequency, distance from transmitter, base station height and reference environment are met.

Based on their theoretical foundation, models can be classified as: *empirical, physical* and *semi-empirical*. Each category is explained in the following paragraphs.

2.3.1 *Empirical models*

Empirical models consist of an analytical formula often used to calculate the average path loss extracted from data. Data is obtained from a comprehensive measurement

campaign, by applying regression algorithms, for example. Its simplicity is both a strength and a weakness, because, on one hand, it makes them very useful in providing a fast evaluation of propagation, but on the other hand, provides a rough comprehension of involved the mechanisms. Their extension is limited due to the dependence of the environments where measures were taken. However, they are site-independent, for environments with similar characteristics to some extent.

2.3.2 *Physical models*

Conversely, physical models rely on the electromagnetic theory and formulas to offer a good and more reliable insight into propagation than empirical counterpart. They are further divided in:

- *Physical-statistical*: the environment is described through statistical parameters. With reference to urban case, mean street width, mean building height, average distance between buildings, etc…
- *Physical-deterministic*: model that requires a complete 3D map of the propagation environment to trace rays and evaluate the field along it.

2.3.3 *Semi-empirical models*

This category includes hybrid-models, based on theoretical solution achieved in some simple and reference cases , then improved by the introduction of empirical correction factors. At the beginning of a design process of radio system, the planner is interested in the coverage area extension and cellular layout, so for this reason, together with empirical models, this model has been conceived as starting point during the design phase because it guarantees a fast and satisfactory prediction.

2.3.4 *Propagation models for FWA*

In the FWA system, where the CPE's antenna is usually placed on the wall close to the roof top or lower, the dominant propagation mechanism in the last part towards the user are reflection, corner and roof-top diffraction. Traditional empirical models are not suitable for FWA applications since they employ free space loss and do not shape reflection and diffraction as they increase the complexity level and the computational

burden. However, failing to consider these mechanism leads to wrong evaluation because they can considerably spoil reception. Therefore, they cannot be ignored.
In this context, there are numerous approaches to properly predict propagation loss. Another way is modelling with ray-tracing techniques that have been widely used for the analysis of radio channel characteristics and systems performance. They usually rely on semi-empirical models, of which the Epstein-Peterson model is one of the most used.

Chapter 3

Measurement equipment and campaign

The antennas' placement plays a significant role in the FWA network planning, affecting the received power and the quality of the offered service. In this phase, the operator has to figure out where to locate the radiating element. For an outdoor solution, it may be necessary to consider whether to place it on the same floor where the user lives, on the roof, possibly in line of sight, or on another face of the same building. Therefore, there are many options available that must be carefully evaluated on a case-by-case basis.

For a correct evaluation, mobile operators perform simulations with dedicated software in order to understand how the reception is at higher positions, typically occupied by the FWA antenna. Existing propagation models widely used by companies are applicable at ground level only, thus, making a correction necessary to extend them to FWA applications as well. In the future, during the design phase, such factor can be used and added to existing propagation models to get an idea of the final attenuation based on the height.

In order to find the correction factor in an empirical way, we raise the antenna's position and see how much the signal improves or worsens by measuring the received field strength, then compared to a reference value on the ground.

The chapter describes everything related to the measurement campaign, as the measurement equipment utilized, the method used for measures and region selection criteria.

3.1 Measurement equipment

The measure consists in the field intensity detection at variable height, which in turn is set by means of an extensible and flexible telescopic barrel of 12 meters long. The source is a set of Base Stations, all equipped with both LTE and 5G NR systems, whose height is approximately 30 meters and cover tri-sectorial macrocells with 8 beams per cell, generated and independently managed by the base stations itself.

The receiving antenna chosen is a linearly polarized dipole with an omnidirectional radiation pattern, inside a black plastic package. In the test, only one component is sufficient for our purposes; we experimented the field reception by placing the antenna vertically first and horizontally then, but we did not notice any significant change, thus, for simplicity, we vertically located it on the top of the rod. The characteristics declared in the datasheet are reported in table 3.1 .

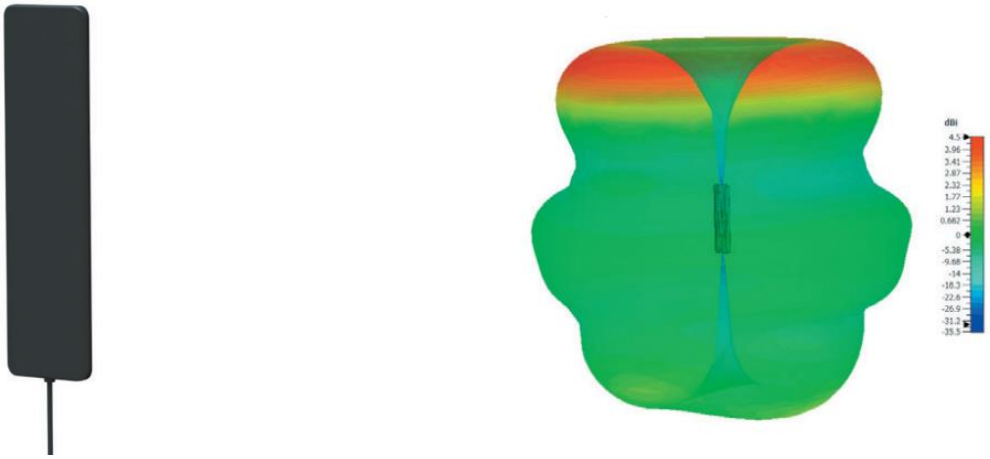

Fig. 3.1: Dipole antenna (left) and radiation pattern at 3.6 GHz (right).

The scanner, designed and developed by Rohde & Schwarz, is a broadband system up to 6GHz remotely connected through Wi-Fi to the operator's pc, used to scan the environment searching for the synchronization signal to start the measure, whose results are then displayed and visible by means of the dedicated software user interface shown in picture 3.2. We can see the following reference signals intensity emitted by all the beams generated by the base station. The official definitions released by the European Telecommunication Standards Institute (ETSI) [6] are also reported:

- SS-RSRP: is the synchronization signal (SS) reference signal received power and is the linear average power, expressed in watt, of the radio resources elements that carry secondary synchronization signals. The measurement's duration is set according to the physical broadcast channel block measurement time configuration (PBCH SMTC).

- SS-SINR: is defined as SS – signal to interference ratio and denotes the ratio between the average received power, in watt, of radio resources elements carrying secondary synchronization signals and the average noise and

interference power contributions, in watt, within the current frequency bandwidth, unless otherwise specified.

- SS-RSRQ: is the secondary SS reference signal received quality, defined as N*SS-RSRP/NR carrier RSSI, where N is the number of resource blocks in the NR carrier RSSI measurement bandwidth. In turn, the denominator is given by the linear average received power, in watt, measured over the OFDM symbol time, over N number of resource blocks from all sources and within the measurement bandwidth.

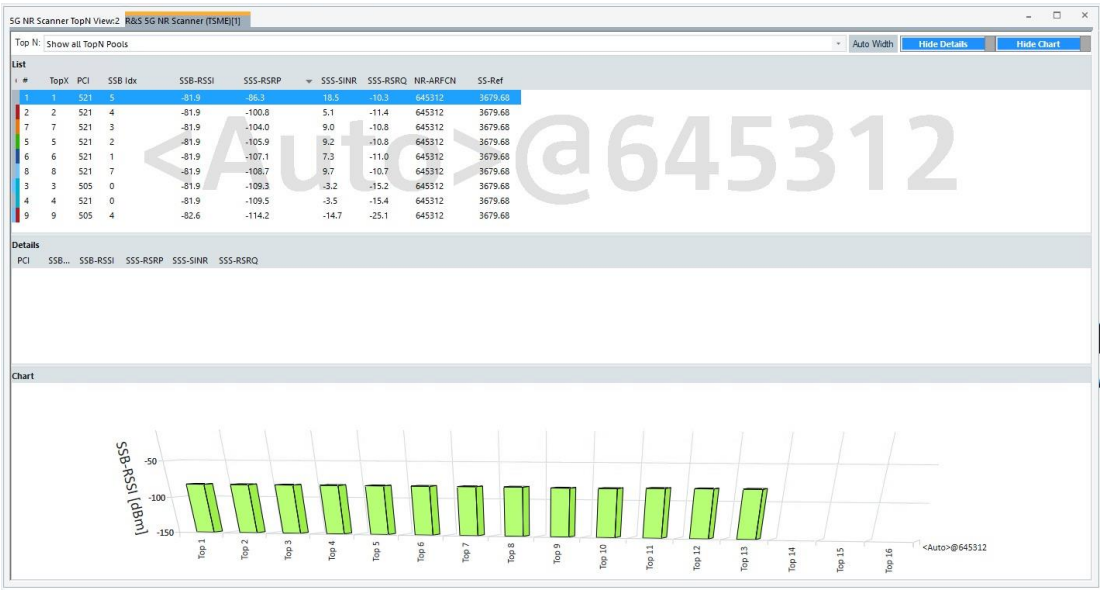

Fig. 3.2: Example of the software's user interface during measurements

Fig. 3.3: Test scanner

The received signal travels the 15 meters long coaxial cable down to the terminal it is connected to. Regarding the wire's attenuation, the information is not written in the device's datasheet for the operative bandwidth, so we empirically computed it by measuring the electric field with wire connected and without it, in this last case the antenna was directly interfaced with the scanner. The difference between the obtained

values provides the cable's attenuation, which is 12.4 dB on average. The following table summarizes devices' meaningful technical aspects.

Reference band	3.4 – 4.2 GHz
Peak isotropic gain	4.5 dBi
Scanner sensitivity	-140 dBm
Scanner sampling rate	4.5 Hz
Typical efficiency	>85%
Polarisation	Vertical
Pattern	Omni-directional
Impedance	50 Ω

Table 3.1: Main antenna's and measurement system's characteristics.

3.2 Measurement campaign

The test was entirely conducted outdoor, within a circular area of about 1km radius from the radio base station, in different provinces between Emilia-Romagna and Lombardy regions. We preferred residential locations with buildings transversally arranged with respect to the base station and already covered by 5G signal, not reached by fiber, but rather by copper line with probably not satisfactory network performances, where operators could evaluate the deployment of 5G FWA applications to offer a better service.

In particular, selected sites are: Reggio Emilia, Modena, Cremona and Ravenna, as depicted in figure 3.4.

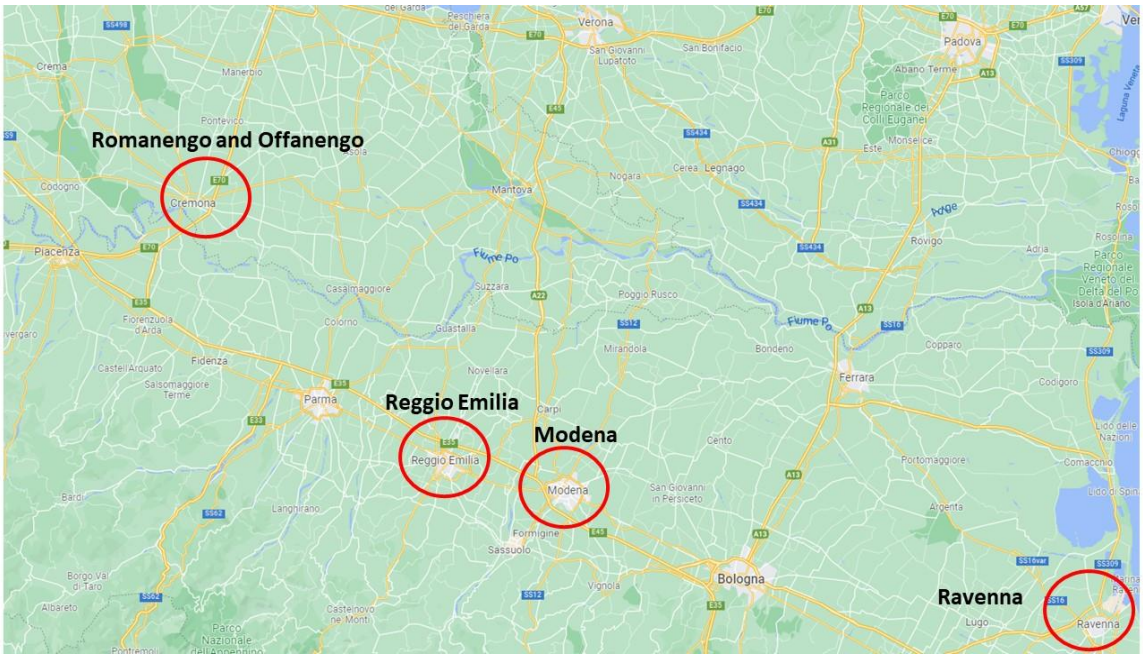

Fig. 3.4: Test sites

The followed method consists of a selection process whereby the points chosen belong to the 3 sectors of the cell. As shown in figure 3.5, for each point, measures were taken at three different positions along a line in steps of 2 meters, so as all the values at same height are then averaged in order to get rid of fast fading effects to some extent.

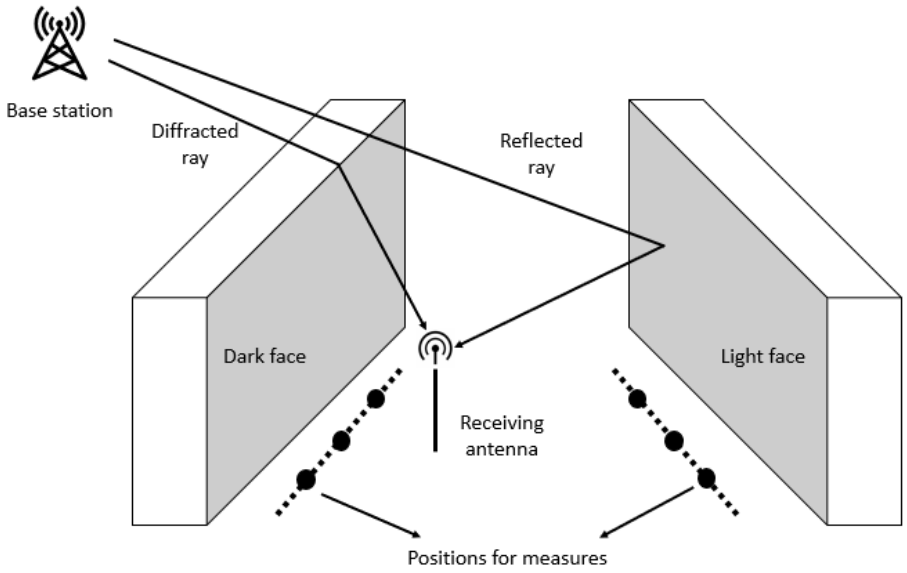

Fig. 3.5: Measurement setup scheme and some meaningful received rays.

For each position and height, we measure the reference signal received power (RSRP), in the 3.6 GHz band, over a temporal window of 90 seconds and storing 405 samples with a sampling rate of 4.5 Hertz, in order to ensure a confidence interval at 98% of 0.462 dB around the mean value, with a standard deviation equal to 4 dB.
We start the recording at 1.5 meters (called A level) from the ground for each location, storing the reference value. Then, the height of the receiving antenna is varied and positioned at predefined heights levels. Afterwards, for each position we repeat the measurement again until we have covered all points. The process is replicated for both the "*light*" and "*dark*" sides, according to the following distinctions we made: the former is the furthest one between the two sides and looks at the base station, whereas the latter is the closest and placed on the opposite side of the light face. Such assumption is important in order to diversify the measurements and to refine the analysis.
Afterwards, recorded values are collected in a file with a label composed of an alphanumeric code where fields are separated by dots as follows:

- Province code: every Italian province has a unique two-letter code for identification. In this case, codes are: CR = Cremona, MO = Modena, RE = Reggio Emilia and RA = Ravenna.
- PCI: operator's cell identifier.
- Test point number: point identification number.
- Face type: specifies whether the measure refers to dark or light side.
- Position number: identify one of the three positions along the line, as stated above.
- Height: a letter defines at which altitude the measure was taken, with reference to the ground. Reference heights are: A = 1.5 m, B = 4.5 m, C = 7.5 m, D = 10.5 m and Z = 12 m.

Below, we can see some pictures taken on field during the measurements so as to show the real measurement setup.

Fig 3.6: Different locations for measurements

Chapter 4

Simulation

The simulation is the process of designing, testing and analysing a model that provides an abstraction of the real physical system under observation.
The benefits are multiple as flexibility, fast design phase, relatively low cost and accuracy, making this approach excellent to observe and analyse information related to the system's operational characteristics in order to better understand the behaviour, to describe it and to predict the evolution over time, allowing the designer to take decisions more easily without having to physically reproduce them but simply setting the input variables, performing the simulation and then observing the effects on output variables.
Nevertheless, when we try to model reality we have to find a reasonable trade-off between the model accuracy and system complexity because they grow together, i.e., the higher the former, the higher the latter, thus it may happen that a very close to reality system could be computationally very hard and/or expensive to be executed.
Therefore, in our case, the goal is to synthesize, with some approximations, a real urban scenario to estimate the floor gain factor along a vertical direction at predefined heights levels. The result is achieved by computing the field along the rays at receiver's side and then computing the difference with the reference value at level A, following the same procedure of the measurement campaign. The simulation also allows to investigate which contributions are more important among those considered and understand how the propagation takes place.
We considered the path from the base station to the final receiver and defined a mathematical model for the simulation that has been conducted by making use of the MATLAB software.
In this chapter, we start from the hypothesis of *incident plane wave* on the building before the receiver and then we move to the description of the rays included in the simulation with related formulas and condition of existence.

4.1 Reference simulation model

The reference model selected for simulation is physical-statistical based on the following important hypothesis:

1. The theoretical foundation is the geometrical theory of propagation that describes the electromagnetic propagation phenomena by means of rays, resulting in an easier and more simplified description, suitable for the final goal.
2. For simplicity, the incident wave is assumed as *plane* with a certain angle of arrival $\alpha > 0$ evaluated with respect to the building placed on the receiver's left side.
3. We focus the attention on the Roof-To-Street propagation, thus we do not consider all the obstacles until the last part of the path and we model both the buildings right before and after the receiver as *knife-edges*.
4. For simplicity, the receiver's antenna is assumed as isotropic at this stage.

All the input variables are presented and described in the following table and shown in picture 4.1:

Variable	**Description**
dbk	Base station – KE distance
ws	Street width
drx	Distance between receiving antenna and building's dark side
hbs	Base station's height
h1	Dark side building's height
h2	Light side building's height
α	Plane wave's angle of arrival
β	Diffraction angle
θ	Angle between the incident shadow boundary and diffracted ray
E0	Incident field amplitude at the first building
n1	Index of refraction of air = 1
n2	Index of refraction of walls = $\sqrt{5}$

Table 4.1: Model's input variables definition.

4.2 *Considered contributions to the total received field*

Generally speaking, the multipath nature of the propagation environment leads us to evaluate the total field as the sum of a multitude of rays reaching the receiver. The rays that appear in the model are:

- Direct ray
- Reflected ray
- Reflected ray of higher orders (2, 3 and 4) due to multiple bounces on walls
- Diffracted ray originated by the building's edge in the middle between the base station and the receiving antenna.
- Diffracted-reflected ray that, after being diffracted, is reflected by the building after the receiver.

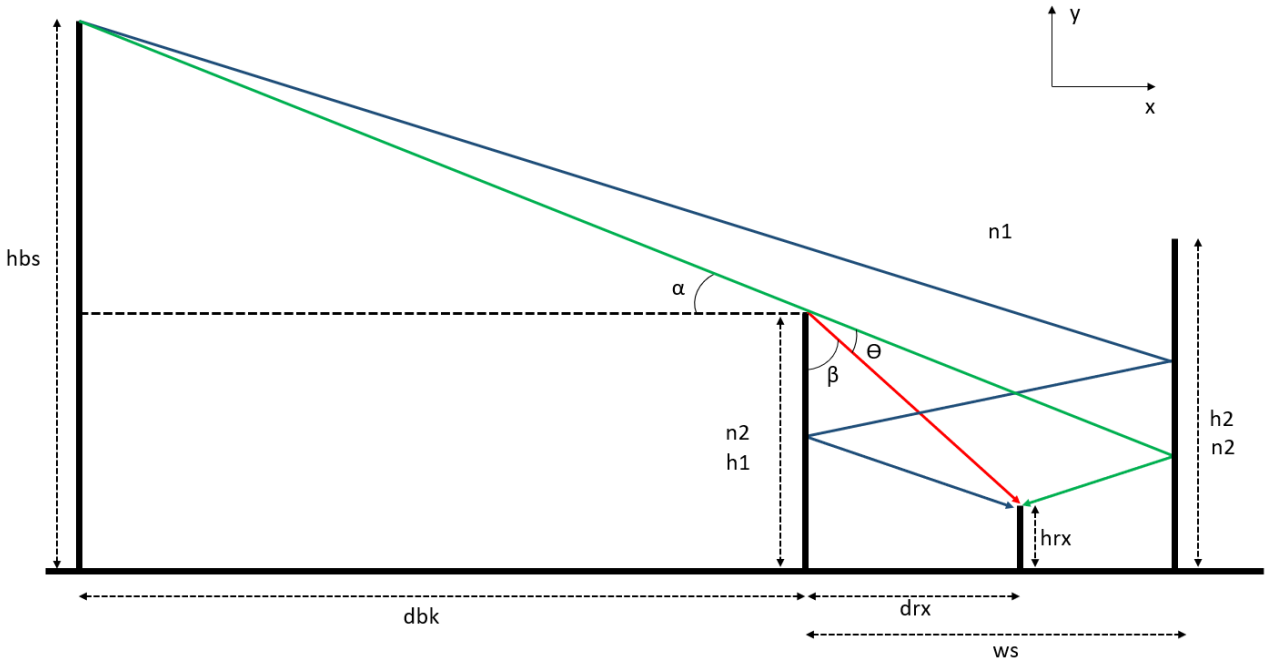

Fig. 4.1: Reference scheme and some propagation mechanisms considered.

The simulation consists of calculating the field along all the aforementioned rays in different situations in order to estimate the floor gain factor, as the difference between actual level (B, C, D or Z) and the value at level A. To calculate the module of the total received field, we can identify two possible approaches: we can compute it in coherent or non-coherent manner.

If we follow the first method, the module of the total field is equal to the sum of all received contributions also considering each phase and, thus, taking into account the

way they interfere. However, accurately predicting the phase of each is quite difficult and inaccuracies in the geometric model can lead to significant prediction errors. Unfortunately, we are not able to know how all the rays are really combined at the time of the measurements in each point, therefore, for simplicity, we opted for the non-coherent method whereby the total field is given by the sum of the module squared of each individual received contribution without considering the phase. Therefore we have:

(4.1) $E_{tot\ dBm} = 10*\log(|E_{direct}|^2 + |E_{reflected1}|^2 + |E_{reflected2}|^2 + |E_{reflected3}|^2 + |E_{reflected4}|^2 + |E_{diffracted}|^2)$

4.3 Direct ray

The direct ray is usually the most powerful contribution to the total field, when present. In order for the receiver to be directly visible, the condition $\alpha > \alpha_1$ must be satisfied, where the direct ray's angle of arrival α is measured clockwise from the horizontal line passing through h1 and touching the ray. The reference geometrical situation is depicted in figure 4.2.

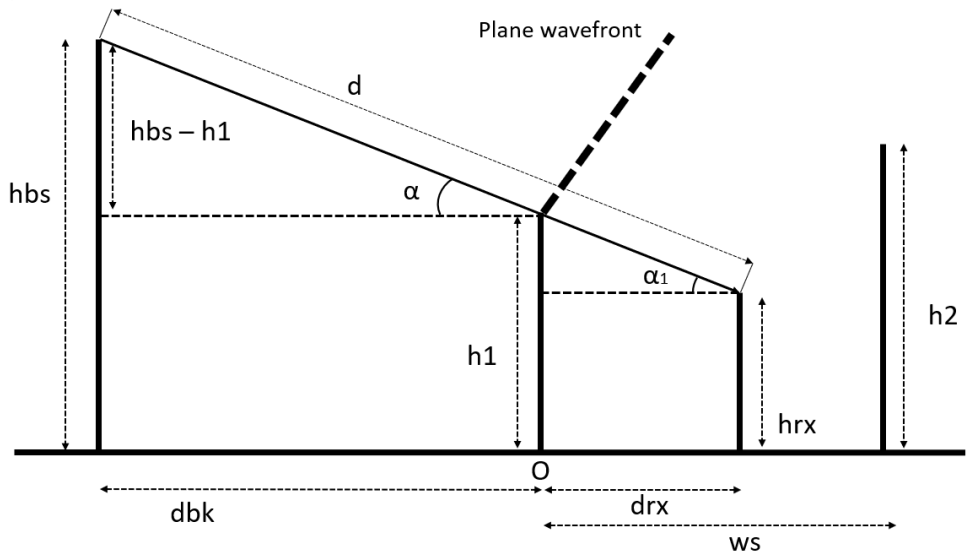

Fig. 4.2: Reference picture for direct ray case

With respect to the figure above, the angles α and α_1 are given by the expressions:

(4.2) $\alpha = arctan(\frac{hbs-h1}{dbk})$ (4.3) $\alpha_1 = arctan(\frac{h1-hrx}{drx})$

The field travelling down the ray is given by:

(4.4) $E_{direct} = E_0 \cdot e^{-j\beta d}$

In the expression (4.4), d is the distance between the receiver and the straight line describing the plane wavefront. Therefore, by considering a (x,y) reference system centred on first building (point O), having y axis along h1 and x along the street towards the right-hand side, then we can write the following equation:

(4.5) $y = m \cdot x + q = tan(90 - \alpha) \cdot x + h_1$

Now, the general expression of d is reported below, but the actual value is obtained by imposing the receiver's coordinates (X_{rx}, Y_{rx}) = (drx, hrx):

(4.6) $d = -\frac{y_{RX} - (m \cdot x_{RX} + q)}{\sqrt{1+m^2}}$

Note that the minus sign in (4.6) takes into consideration the field's phase change according to the receiver's position with respect to the plane associated to the wave. Indeed, when the receiver lies above such plane, d is negative and the wave is in advance, first touching the receiver then the building h1. On the contrary, when the receiver lies below, d is positive and the wave is delayed.

4.4 Reflected ray

In the absence of the strongest contribution, reflection can make the difference, so not considering it would lead to an underestimation of the received field. Reflections of orders two, three and four have also been included in our model.

We can apply the image principle, by placing the image receiver with respect to the second building as shown in the following reference scenario:

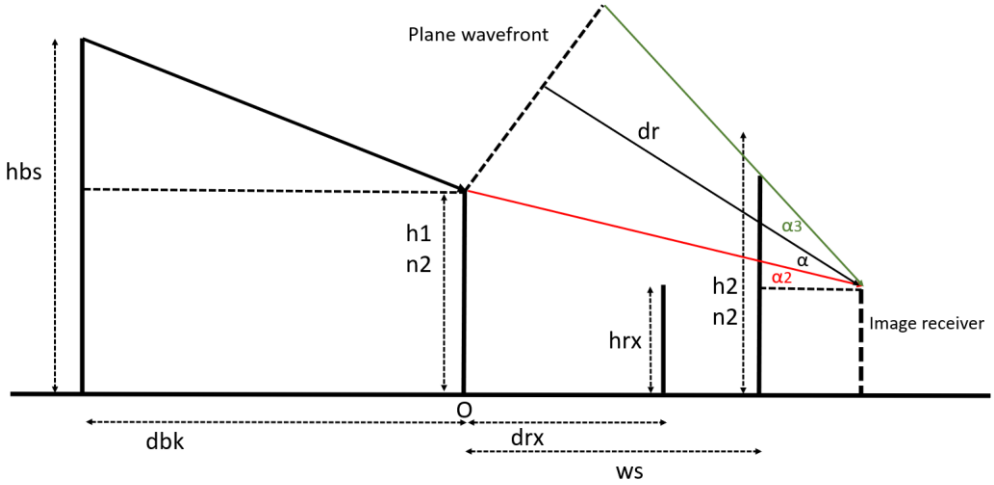

Fig 4.3: Reference scenario for reflected ray

Two conditions must be satisfied for the existence of the reflected ray:

I. the image receiver is directly visible from the incident wave (if we do not consider the second building), that is the angle of arrival must be in agreement with $\boldsymbol{\alpha > \alpha_2}$, where α_2 is equal to:

$$\alpha_2 = arctan\left(\frac{h_1 - h_{RX}}{(2ws - d_{RX})}\right) \quad (4.7)$$

II. the ray starting from the incident wavefront and goes towards the image receiver with coordinates (X_{rx}, Y_{rx}) = (2ws - drx, hrx) must intersect the second building as shown in picture 4.3, thus $\boldsymbol{\alpha < \alpha_3}$, with α_3 equal to:

$$\alpha_3 = arctan\left(\frac{h_2 - h_{RX}}{(ws - d_{RX})}\right) \quad (4.8)$$

The reflection coefficient is a complex number that depends on incident angle and refraction indexes. In order to correctly calculate it, we have to consider the electric field is vertically polarised, therefore we are in the TM case with respect to the incident wall of the second building. We can write it as:

$$\Gamma_{TM} = \frac{\cos(\theta_i) - \left(\frac{n1}{n2}\right) * \sqrt{\left(1 - \frac{n1}{n2}\right)^2 - \sin(\theta_i)^2}}{\cos(\theta_i) + \left(\frac{n1}{n2}\right) * \sqrt{\left(1 - \frac{n1}{n2}\right)^2 - \sin(\theta_i)^2}} \quad (4.9)$$

The reflected field along the ray is:

(4.10) $E_{reflected} = \Gamma_{TM} \cdot E_0 \cdot e^{-j\beta d_r}$

We evaluate the length d_r as the distance along the ray between the wavefront and the image receiver. The value is given as done in direct ray case, therefore m = tg(90 - α), q = h1 and imposing the image receiver's coordinates into the expression (4.6).

4.5 Ray reflected twice

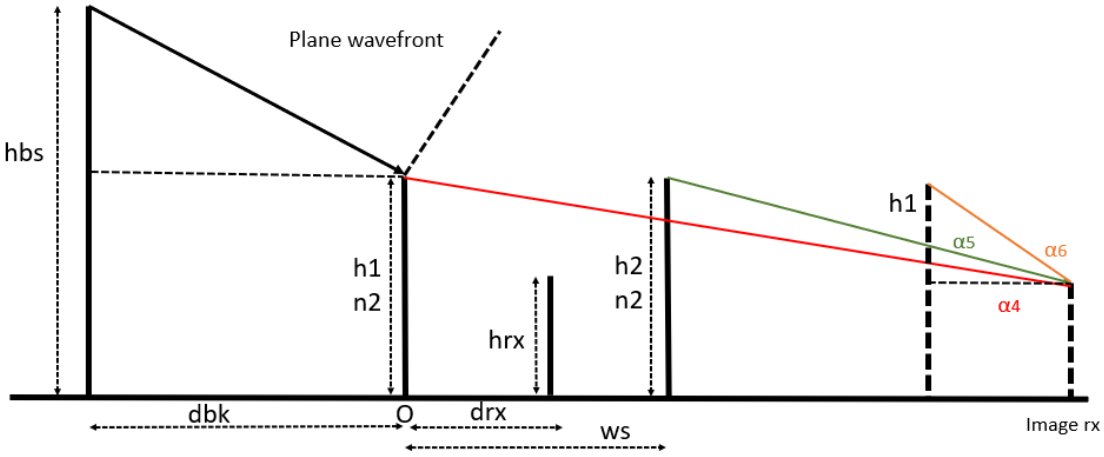

Fig. 4.4: Double reflected ray reference scheme

We can extend the image principle to this case too that leads to the geometrical reference case depicted in figure 4.4.
Similarly, the doubly reflected ray exists when the straight line crosses the building in the light side and the image of the building in the dark side, finally arriving at the image receiver of coordinates (X_{rx}, Y_{rx}) = (2*ws +drx, hrx).
Regarding the condition of existence, in this case we have to say that: the statements I and II, properly adapted, are valid also in this case. Therefore we have, where:

I. The virtual receiver is visible by the ray, without considering the building 1 and 2 as depicted in image 4.4, therefore $\alpha > \alpha_4$:

(4.11) $\alpha_4 = arctan(\frac{h_1 - h_{RX}}{(2ws + d_{RX})})$

II. The ray must intersect the building in light condition and this implies that $\alpha < \alpha_5$, where α_5 is given by:

(4.12) $\alpha_5 = arctan(\frac{h_2 - h_{RX}}{(ws + d_{RX})})$

III. The ray must intersect the image of the building in dark condition. As a consequence, $\alpha < \alpha_6$, where α_6 equal to:

(4.13) $\alpha_6 = arctan(\frac{h_1 - h_{RX}}{drx})$

The field along the ray reflected twice is:

(4.14) $E_{reflected\_2} = \Gamma_{TM}^2 \cdot E_0 \cdot e^{-j\beta d_{r2}}$

Analogously, the distance d_{r2} is calculated by imposing the image's receiver coordinates into the expression (4.6), considering that m and q parameters are the same of the reflected ray.

4.6 Ray reflected three times

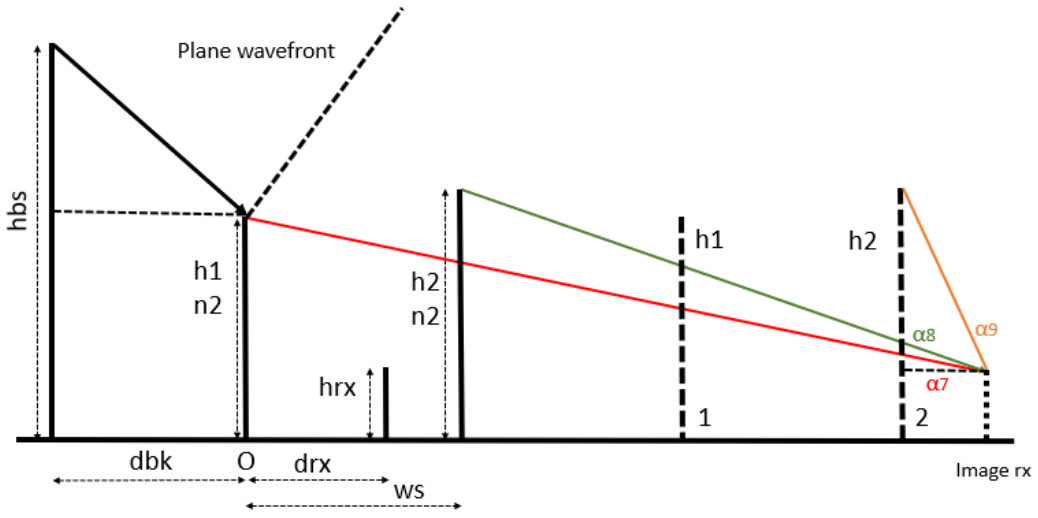

Fig. 4.5: Ray reflected three times reference scheme

Also in this case, we can apply the image principle, obtaining the geometrical situation shown in figure 4.5.

As done previously, the ray reflected three times exists only when the straight line, with slope equal to the angle α, crosses the second building and the sequence of image buildings 1,2 and finally reaches the image receiver, whose coordinates are (X_{rx},Y_{rx}) = (4*ws - drx, hrx).

Adapting the statements I, II and III to this case, the condition of existence is $\alpha_7 < \alpha < \alpha_8 < \alpha_9$, where:

(4.15) $\alpha_7 = arctan(\frac{h_1 - h_{RX}}{(4ws - d_{RX})})$

(4.16) $\alpha_8 = arctan(\frac{h_2 - h_{RX}}{(3ws - d_{RX})})$

(4.17) $\alpha_9 = arctan(\frac{h_2 - h_{RX}}{(ws - d_{RX})})$

The field along the ray reflected three times is:

(4.18) $E_{reflected\_3} = \Gamma_{TM}^3 \cdot E_0 \cdot e^{-j\beta d_{r3}}$

Replacing (x,y) with image receiver's coordinates in (4.6), we obtain the distance d_{r3} from the wavefront along the ray.

4.7 Ray reflected four times

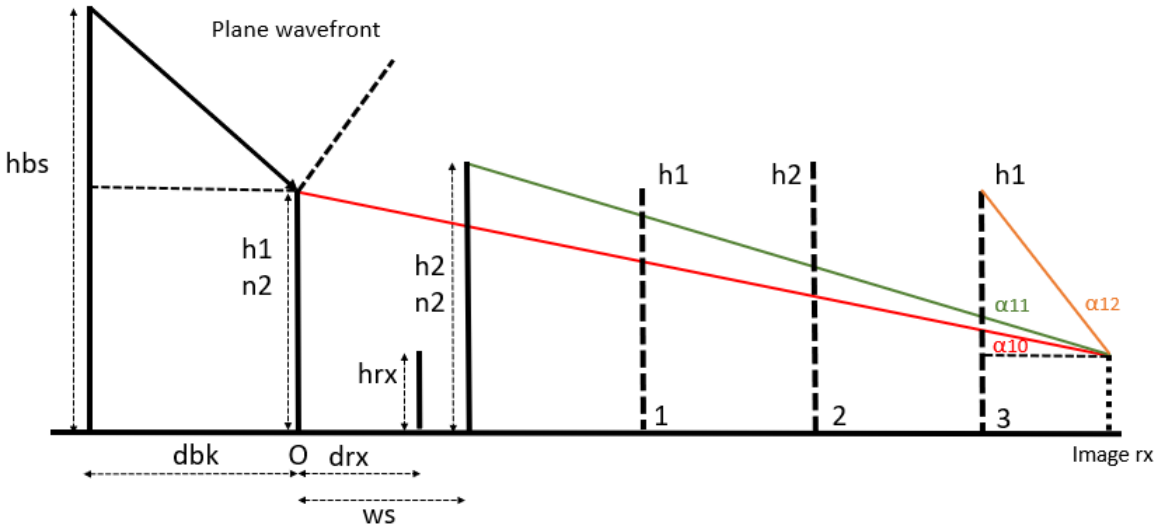

Fig. 4.6: Ray reflected four times reference scheme.

Analogously as previous paragraph, we can state that the ray reflected four times exists when the related straight line crosses the second building, the image buildings 1,2,3 and finally reaches the receiver with coordinates (X_{rx},Y_{rx}) = (4*ws + drx, hrx).
Adapting the statements I, II and III to this case, the condition of existence is $\alpha_{10} < \alpha < \alpha_{11} < \alpha_{12}$, where:

(4.19) $\alpha_{10} = arctan(\frac{h_1 - h_{RX}}{(4ws + d_{RX})})$

(4.20) $\alpha_{11} = arctan(\frac{h_2 - h_{RX}}{(3ws + d_{RX})})$

(4.21) $\alpha_{12} = arctan(\frac{h_1 - h_{RX}}{drx})$

The field along the ray reflected three times is:

(4.22) $E_{reflected\_4} = \Gamma_{TM}^{4} \cdot E_0 \cdot e^{-j\beta d_{r4}}$

Yet again, by replacing (x,y) with image receiver's coordinates in (4.6), we can calculate the length d_{r4} along the ray.

4.8 Diffracted ray

In order to proceed with the diffracted ray, we can consider the reference geometrical scenario reported below:

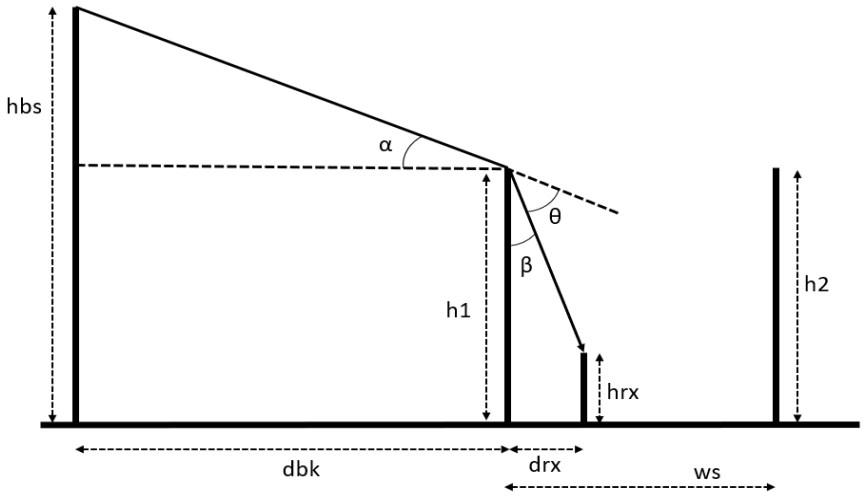

Fig. 4.7: Diffracted ray reference scheme.

Unlike before, the diffracted ray is always present and created when the incident plane wave impacts on the knife edge causing the generation of a cylindrical wave. The diffracted ray propagates from the top of the first building down to the receiver, with a slope equal to the diffraction angle β.
The angle θ is the angle between *incidence shadow boundary* (ISB) and the diffracted ray, with a positive value when located below such boundary (case A) and negative otherwise (case B), therefore we have to distinguish two different situations:

(4.23) $\theta = \begin{cases} 90 - \alpha - \beta \ \ if \ \ y_{RX} \leq m \cdot x_{RX} + q \ (case\ A) \\ -(90 + \alpha - \beta) \ if \ \ y_{RX} > m \cdot x_{RX} + q \ (case\ B) \end{cases}$

With (X_{rx},Y_{rx}) = (drx, hrx), m = tan(α) and q = h1. The diffraction angle β is:

(4.24) $\beta = arctan(\frac{d_{RX}}{|h_1 - h_{RX}|})$

The final expression for diffracted field over the ray of length d_d is:

(4.25) $E_{diffracted} = \frac{E_0 \cdot D(\theta) \cdot e^{-j(kd_d + \pi/4)}}{\sqrt{d_d}}$ (4.26) $d_d = \sqrt{(h_1 - h_{RX})^2 + d_{RX}^2}$

The term D(θ) is the Bertoni's diffraction coefficient, a scalar number and valid for plane waves, whose expression is:

(4.27) $D(\theta) = -\frac{1+\cos(\theta)}{2\sin(\theta) \cdot \sqrt{2k\pi}} \cdot F(s)$

Note that F(s) is called *transition function* and it was first introduced in the uniform theory of diffraction to solve the problem due to the singularity at the shadow boundaries:

(4.28) $F(S) = 2j\sqrt{S}e^{js} \int_{\sqrt{s}}^{\infty} e^{-ju} du$

(4.29) $S = j\frac{k\rho}{2} \tan(\theta)^2$ with $\rho = d_d$

In the simulation, we cannot implement the integral formula since it is computationally very hard, therefore we decide to impose F(s)≈1 when the angle θ > 5 degrees,

otherwise the function takes an appropriate value to compensate the discontinuity, with a value given by the simplified expression (4.30), reported in the book [7] written by H.L. Bertoni:

(4.30) $F(S) = \sqrt{2\pi S}[\, f(\sqrt{2S/\pi}) + jg(\sqrt{2S/\pi})\,]$

Where:

(4.31) $f(\xi) = \dfrac{1+0.926\xi}{2+1.792\xi+3.104\xi^2}$

(4.32) $g(\xi) = \dfrac{1}{2+4.142\xi+3.492\xi^2+6.670\xi^2}$

4.9 Diffracted-reflected ray

The geometrical situation is reported in figure 4.8:

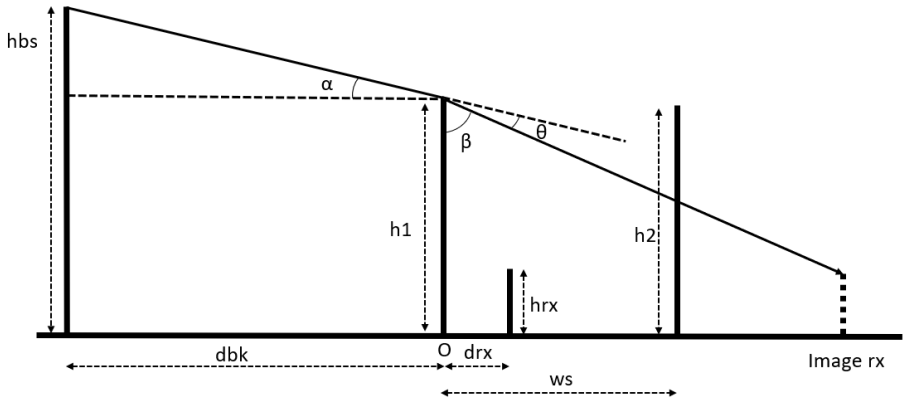

Fig. 4.8: Diffracted-reflected ray reference scheme

This contribution is present as along as the segment, starting from the top of h1, ending at the image receiver, intersects the second building. That is:

(4.33) $Y_2 > m \cdot X_2 + q$

where $(X_2, Y_2) = (ws, h2)$ and $q=h1$.
There are two different cases because the antenna can be lower or higher than building h1. This leads to the following expression for parameter m:

$$m = \begin{cases} tan(90 + \beta) \;\; if \;\; h_{RX} < h_1 \\ tan(90 - \beta) \;\; if \;\; h_{RX} > h_1 \end{cases}$$

The diffraction angle and ray's length d_{dr} are given by:

(4.34) $\beta = arctan(\frac{2ws - d_{RX}}{|h_1 - h_{RX}|})$ (4.35) $d_{dr} = \sqrt{(h_1 - h_{RX})^2 + (2ws - d_{RX})^2}$

Finally, the expression of the diffracted field along the ray is:

(4.36) $E_{diffr} = \Gamma \cdot E_0 \cdot e^{-j\frac{\pi}{4}} \cdot \frac{e^{-jkd_{dr}}}{\sqrt{d_{dr}}} \cdot D(\theta)$

The diffraction coefficient and transition function expressions are given by (4.27) and (4.30) respectively, considering $\rho = d_{dr}$.

Chapter 5

Roof-To-Street data analysis and discussion

In FWA network planning, the antenna's placement is crucial and the operator must find a suitable location for best service performances; therefore a correct evaluation is needed. Usually, the operator performs a simulation, relying on propagation models that usually provide the path-loss at street level. This assumption is no longer true in FWA applications, hence we have to change this paradigm and introduce an additional gain factor, called floor gain factor, for existing propagation models in order to get an idea of the final attenuation based on the height. This is the project's major goal and for this reason we planned the measurement campaign. In this section, the acquired experimental data is described and analysed to statistically evaluate such factor.
For completeness, we also performed a simulation of the propagation model, described in chapter 4, that facilitates and clarify the investigation in the roof-to-street scenario under study with some approximations. Also in this case, the simulator's outcome is presented and analysed in order to finally move on the empirical and theoretical data comparison.

5.1 Measured data and analysis

As mentioned in chapter 3, we connected the scanner to a GPS on the ground and measured the received signal strength from the best beam at level A and then compared with those at the others height levels, with reference to the same beam index. The measure takes about 90 seconds and stores the samples in a specific text file the system creates every time we start a new scan. As seen, the file's name has a particular composition containing what we need to identify the place it refers to and the measure index number. The included information is organized in columns in the following order: time – latitude – longitude – height with respect to sea level – received signal intensity from beam 0…beam 7 – cell's PCI corresponding to the beam with the strongest signal strength – strongest signal intensity measured.
Such data is then processed by executing a script with *gawk*, the GNU/Linux implementation of *awk* programming language, designed to optimize the text processing, thus making this operation faster than conventional languages as C. The

script calculates the signal's mean and standard deviation for each beam, going through all samples, obtaining the output as shown in the image 5.1.

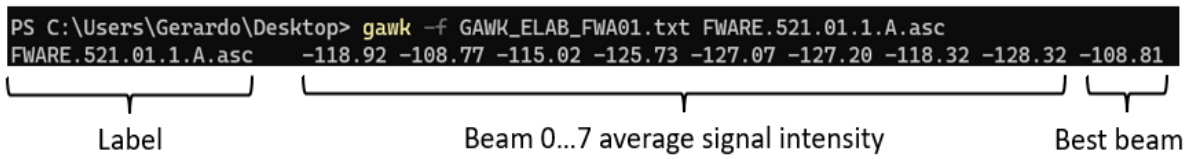

Fig. 5.1: Example of script's output.

We repeat the same procedure over all measured points, then the output is written in an Excel file for further computation. In particular, here we calculate some variables of great interest for the project's purposes, as:

- Label: height with respect to the ground level.
- Mean of standard deviation of best beam: the variable is the average standard deviation over all points. Particularly, for each measured point we calculate the standard deviation that describes the signal's variability around its mean value. Therefore, the lower the value, the more stable the overall signal is. This could be a very useful information during the FWA system design phase since it gives us an idea about where it would be more convenient to place the FWA equipment.
- Average floor gain factor: is the most important data and represents on average the difference between the signal intensity at height indicated in the first column and that of ground level (A).

The table 5.1 visualizes the average values of variables described above:

Height	**Mean standard dev. BestBeam [dB]**	**Average floor gain factor [dB]**
A (1.5 m)	3,46	0,00
B (4.5 m)	3,85	2,60
C (7.5 m)	4,26	4,28
D (10.5 m)	4,15	4,48
Z (12 m)	3,39	12,73

Table 5.1: Statistics of measurements at different heights.

We also made the distinction of dark and light side in order to further differentiate the measures and see how the floor gain factor changes over height for each case.

By separating the first dataset from the second one, we obtain the results reported in tables in figure 5.2:

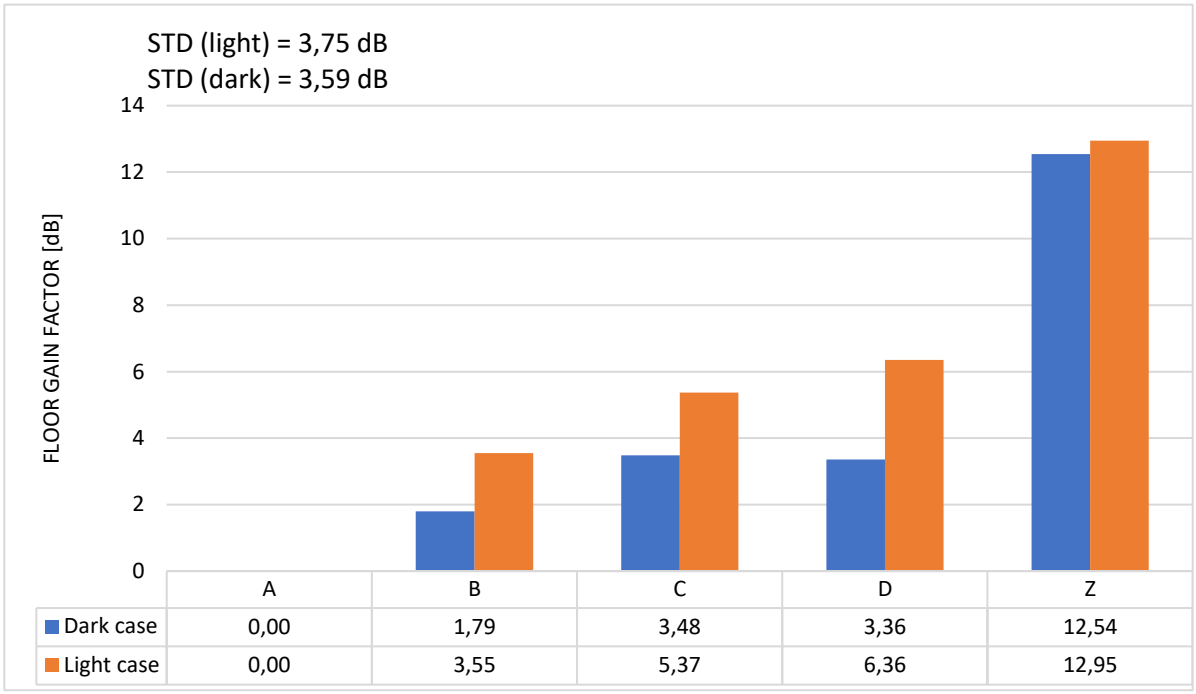

	A	B	C	D	Z
Dark case	0,00	1,79	3,48	3,36	12,54
Light case	0,00	3,55	5,37	6,36	12,95

Fig 5.2: Dark and light cases compared

If we observe the figure above, we realize that the expected trend has been confirmed. The light case is characterized by the largest increment but the signal is slightly more unstable while the dark case by the smallest increase with bit more stable signal.
So, when possible, it is more convenient to place the FWA antenna on light side, since it benefits from better dynamics. However it doesn't mean that the signal intensity is higher than dark case. In order to see which side is better in terms of received power, we can have a look to picture 5.3 , that displays the difference between the received power on light side and that of dark side, for each height level.

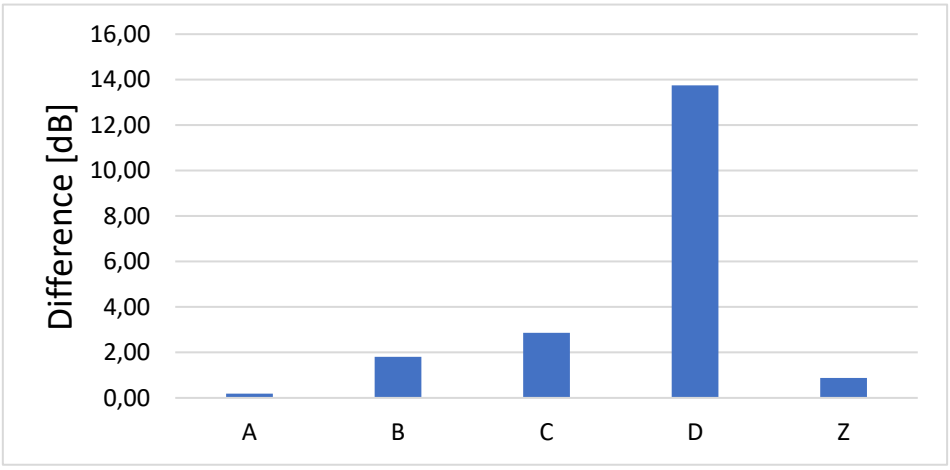

Fig. 5.3: ifference between received power light and dark.

The figure emphasizes the difference is always positive and with increasing value from A to D, denoting that the light case gets more power ad benefits from higher dynamics than dark case.

5.2 Simulation results and analysis

The simulator has been developed by transposing the formulas of GTP theory into code by means of the tools offered by MATLAB. Once the simulation is run, we are able to see how each computed parameter evolves case by case, offering the opportunity to analyse each situation and derive important information on how the propagation mechanism affects the floor gain factor, that otherwise would be hard to see in reality. For this purpose, we first simulate such factor in both dark and light cases, as reported in figure 5.4.

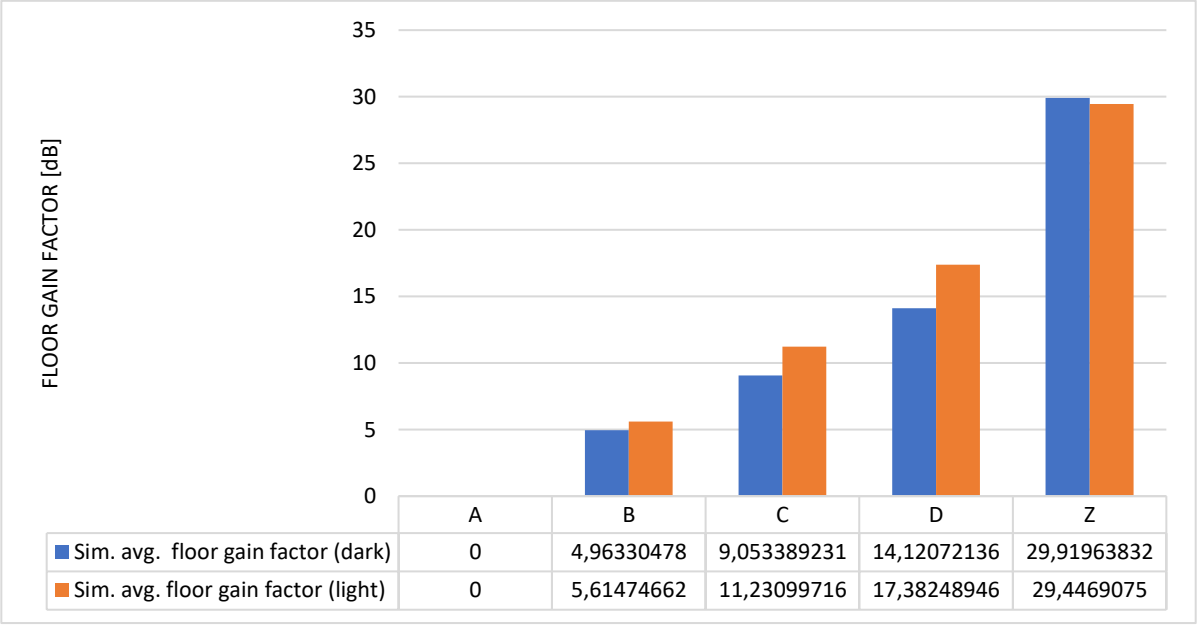

	A	B	C	D	Z
Sim. avg. floor gain factor (dark)	0	4,96330478	9,053389231	14,12072136	29,91963832
Sim. avg. floor gain factor (light)	0	5,61474662	11,23099716	17,38248946	29,4469075

Figure 5.4: Simulated average floor gain factor for dark and light cases

By observing the picture, we realize that the floor gain factor increases with increasing height, evaluated with respect to the ground level, thus being in agreement with the trend found from measurements.
In the simulation, we can isolate each ray to see the impact on the total received field intensity and somehow determine which measure it interferes, for a given height in the roof-to-street environment under study. For this purpose, we calculated the weight of each ray as:

(5.1) $$W_i = \frac{|E_i|^2}{|E_{total}|^2}$$

Since we have measured the received power, in the expression (5.1) it makes sense to focus on the square module. In particular, the numerator is the i-th contribution considered in the model, while the denominator is related to the total received field.
The aforementioned weights for the two possible scenarios are depicted in figures 5.4 and 5.5, emphasising the diffraction and diffraction-reflection as dominant contributions, that interfere with each other from A level to D level, when generally the receiver is obscured by buildings for the two cases studied.
The simulation also denotes the Z level, when the receiver is in line of sight, as the best case because the direct ray becomes the most important component whereas the other ones are negligible, thus producing less interference.
Lastly, reflections are the least significative contribution in almost all cases. The reason behind this statement is related to the reflected ray's condition of existence. Indeed, the requirements are met in a much lower number of cases than diffraction, which in turn is always present. Consequently, reflections have a less statistical impact than other contributions when computing the average over all cases.

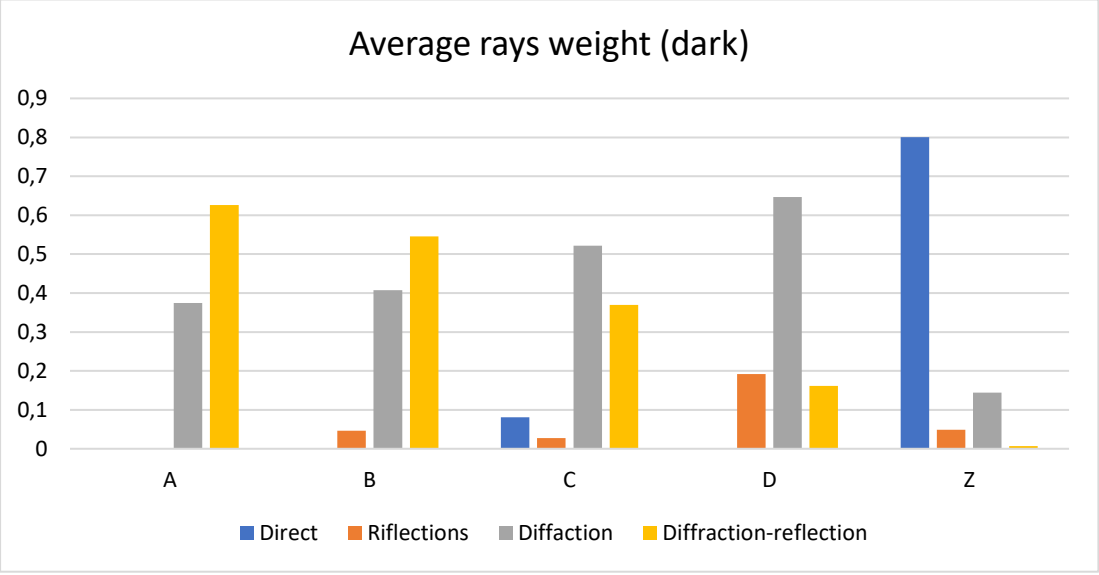

Fig 5.5: Average ray weights (dark case)

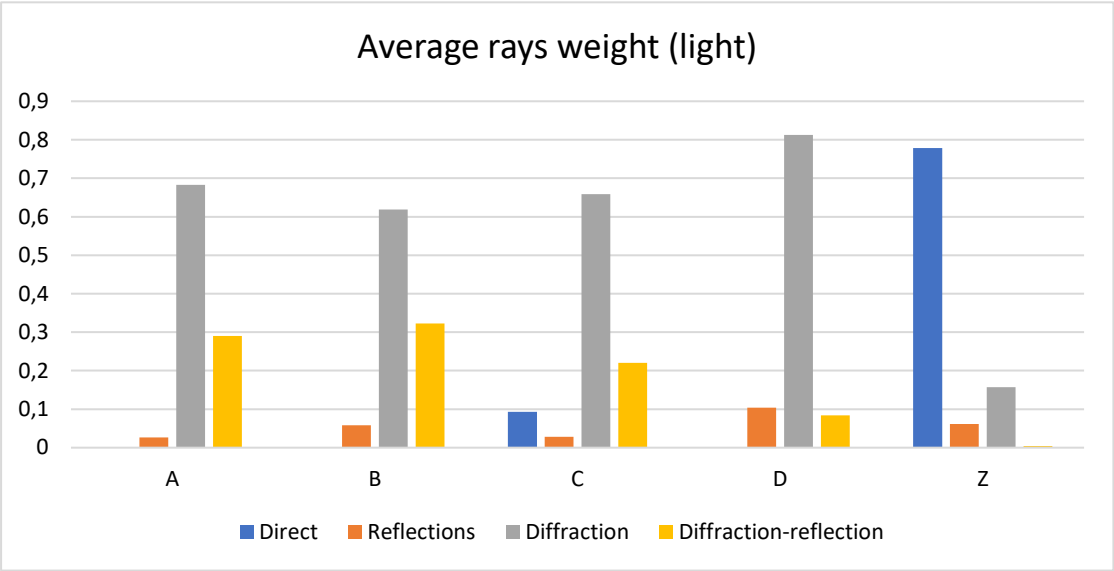

Fig 5.6: Average ray weights (light case)

5.3 Data comparison and discussion

To perform a quantitative comparison with empirical data, it is crucial to calculate the statistical error of the model in relation to the measured values. The mean error, expressed in decibels, is given by:

$$(5.2) \quad \bar{\varepsilon} = \frac{1}{N} \cdot \sum_{i=1}^{N} (y_{model} - y_{measure})$$

Accordingly, we can also compute the root mean square error (RMSE) value to assess the performance of the predictive model. The RMSE is provided by:

$$(5.3) \quad \varepsilon_{RMSE} = \sqrt{\frac{1}{N} \cdot \sum_{i=1}^{N} (y_{model} - y_{measure})^2}$$

In both expressions (5.2) and (5.3), the quantities y_{model} and $y_{measure}$ are the simulated and measured floor gain factors respectively. In our case, we got a mean error $\bar{\varepsilon}$ = 6.269 dB that indicates that the simulated model over-predicts the actual average floor gain factor. Concerning the RMSE value, we obtained ε_{RMS} = 9.98 dB. We can also plot the mean error and RMSE values for each city involved in the measure campaign, to have a better insight of their behaviour:

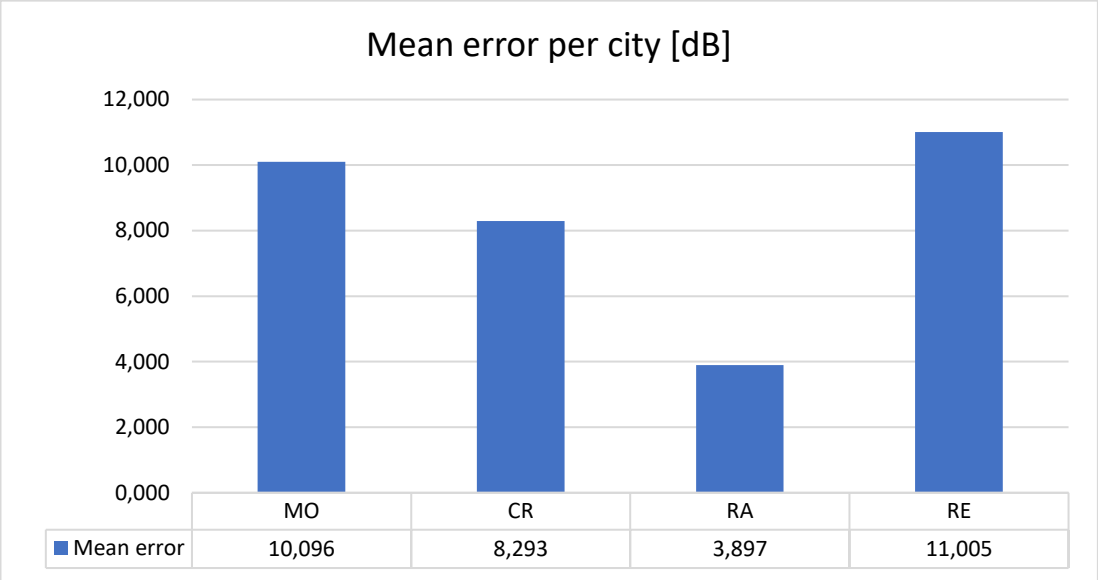

Fig. 5.7: Mean error per city

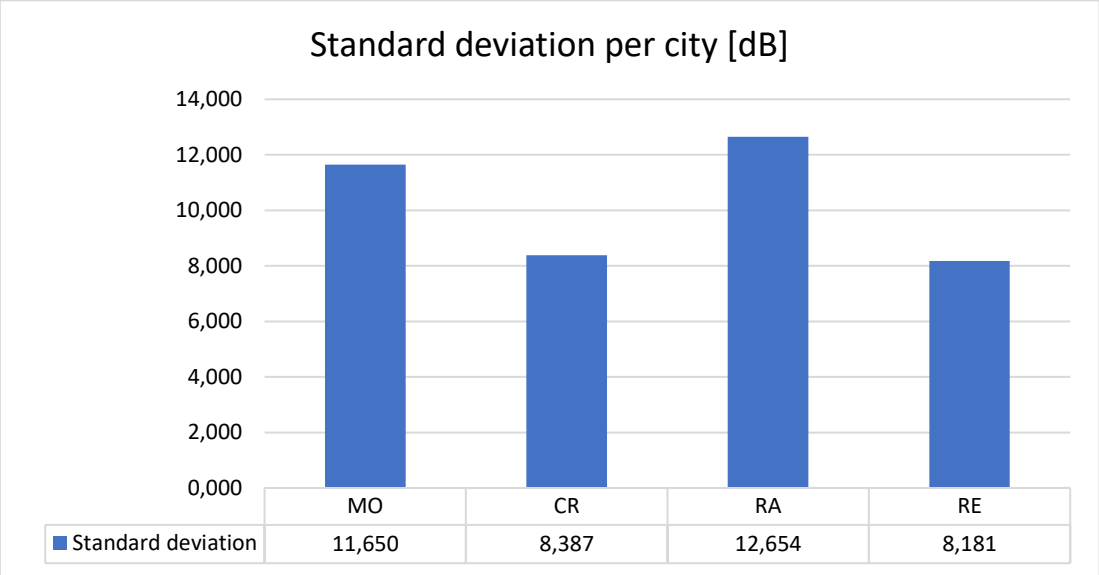

Fig. 5.8: Standard deviation per city

Figueres 5.7 and 5.8 depict the mean error and standard deviation as computed in (5.2) and (5.3). If we consider the hypothesis the propagation model is based on, we can state that the model predicts the floor gain factor better in Reggio-Emilia (RE) city with a mean error equal to 3.897 dB. The reason would be due to the residential areas involved in measurements are generally characterized by low-building profiles, thus less obstruction and shadowing effect; therefore closer scenario to that of described by the model.

Figures 5.9 and 5.10 show the average floor gain factor over different height levels, by matching the measured values with those simulated.

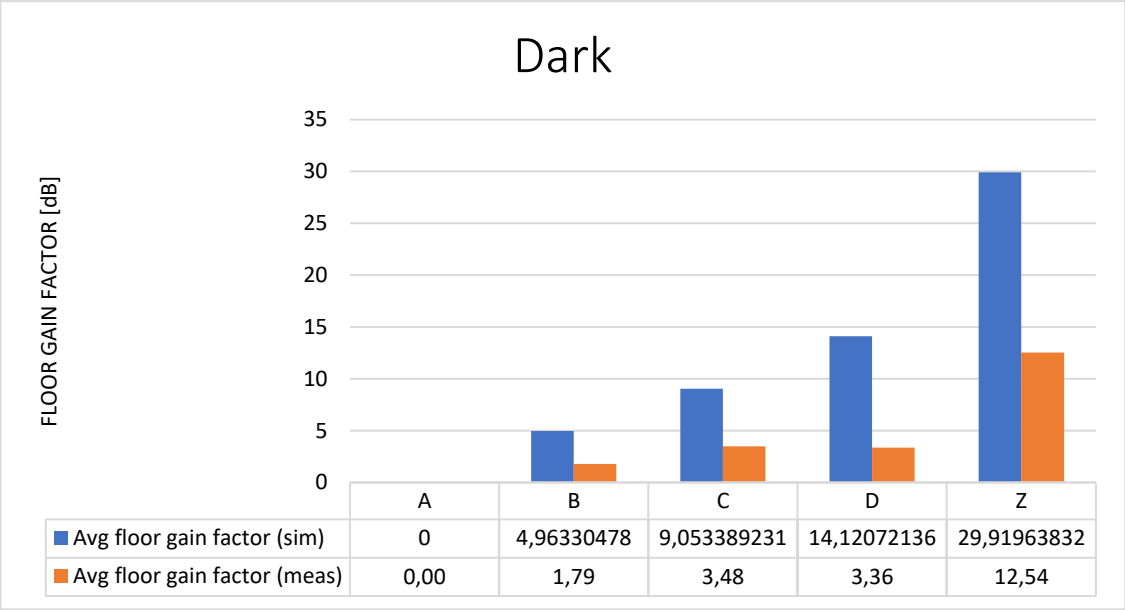

	A	B	C	D	Z
Avg floor gain factor (sim)	0	4,96330478	9,053389231	14,12072136	29,91963832
Avg floor gain factor (meas)	0,00	1,79	3,48	3,36	12,54

Fig. 5.8ù9: Average floor gain factor simulated versus measured, dark case.

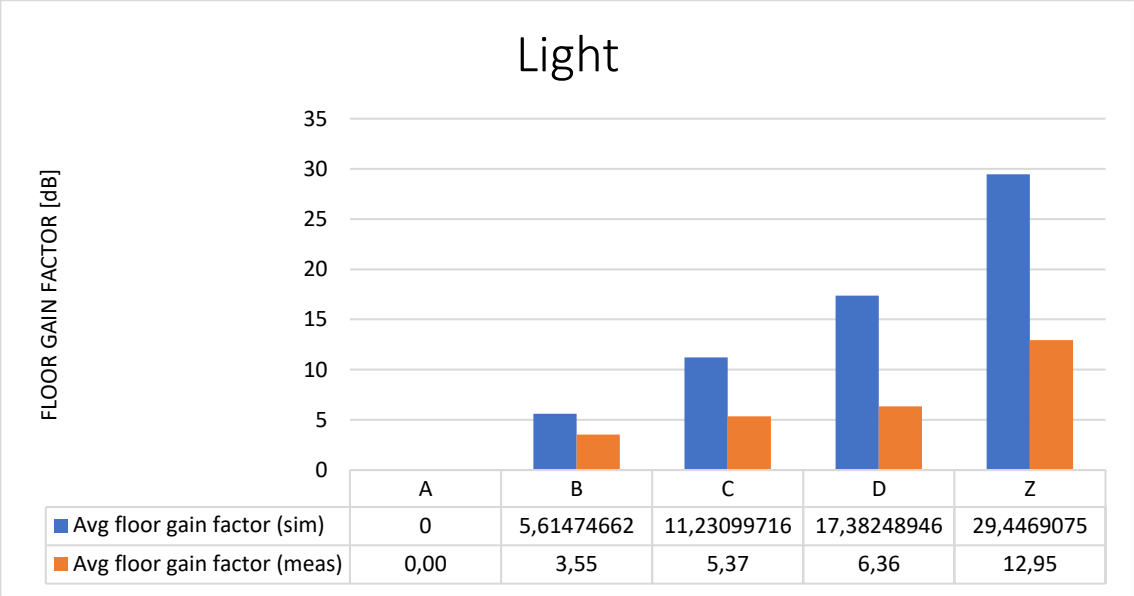

	A	B	C	D	Z
Avg floor gain factor (sim)	0	5,61474662	11,23099716	17,38248946	29,4469075
Avg floor gain factor (meas)	0,00	3,55	5,37	6,36	12,95

Fig. 5.10: Average floor gain factor simulated versus measured, light case.

Both graphs show that the simulator seems less adequate to predict the signal gain by raising the antenna, when the receiver is in line of sight. On one hand, the estimated signal intensity at level A is lower than it actually is. The discrepancy between simulation and reality is due to the model's limitations as we include a restricted

number of rays, though in reality many more are present, which in turn partially compensate this lack, thus resulting in a dynamics not always accurate and generally overestimated. On the other hand, the error is related to the model's inaccuracy about building's roof description because we assumed all of them as flat when in reality they are very likely sloping. Therefore, the higher the slope is, the greater the error committed.

Finally , we assume the receiving antenna as isotropic with same gain for all directions of arrival but this hypothesis does not match reality, leading to an incorrect evaluation. In a future work, this problem could be solved by introducing a proper antenna's gain function that depends on its radiation pattern.

Conclusions

The core part of the present work is the definition of the correction factor, called floor gain factor, based on height evaluated with respect to the street level, to modify existing models in order to predict, to some extent, the propagation mechanism, required for the correct antenna's placement on buildings in FWA applications. To this end, a measurement campaign was conducted to statistically determine such value, on the basis of on-site data collected along two building's sides: dark face, usually the main source of diffraction and light face, located on the opposite side. We selected residential areas of different types and sizes, travelling over several towns of north Italy. The hardware setup is composed of a broadband scanner compatible with new 5G NR technology, tuned on 3.6 GHz frequency band, connected to a receiving antenna placed on the top of an extensible rod. As expected, the empirical data confirms the floor gain factor's increment by raising the antenna with respect to the ground, by a quantity equal to 4.29 dB on average along the dark side and 5.40 dB on average along the light side.

In addition, a model based on the GTP was defined and developed in MATLAB, in order to estimate the floor gain factor and to investigate the problem more deeply. According to the model, the received total field intensity is given by seven contributions: direct ray, single and multiple reflections, diffracted ray and diffracted-reflected ray. Simulated results demonstrated the trend found through experiments and the average floor gain factor increases by 11.61 dB in the dark case and by 12.74 dB in the light case. Moreover, for both dark and light cases, the simulation reveals that diffraction and diffraction-reflection are the main propagation phenomena, rising the interference, when the receiver is not in line-of-sight. On the other hand, if the roof is crossed or when the receiver is in line-of-sight with the base station, their influence on the total received signal drops giving rise to less interference and the direct ray becomes the dominant component.

Reflections seem not to be of meaningful importance, since the related conditions of existence are not always met and, when they appear, multiple interactions cause higher losses and thus lower related weights.

We also compared the simulated and measured gain factor finding that the mean error is 6.269 dB and the mean standard deviation is equal to 9.98 dB.

Finally, we realized the highest discrepancy between simulation and measurements appears at Z level and this could be due to the measurements process and model inaccuracies.

Bibliography

[1] Kudret Topyan, Mehmet Ulema: "*Architectural and financial considerations for deploying 5G based Fixed Wireless Acccess*", 2020, IEEE.

[2] Szymon Izydorek, Annie Gravey, Reza Tadayoni: "*How, when and where can Fixed Wireless Access compete with FTTH*", 2019, IEEE.

[3] Elena Madalina Oproiu, Iulian Gimiga, Ion Marghescu: "*5G Fixed Wireless Access – Mobile Operator Perspective*", 2018, IEEE.

[4] Huawei Technologies Co., "*4G/5G FWA Broadband White Paper*", 2019.

[5] International Telecommunication Union, "*Digital Inclusion of All*", April 2021, https://www.itu.int/en/mediacentre/backgrounders/Pages/digital-inclusion-of-all.aspx

[6] European Telecommunication Standards Institution (ETSI), "*5G NR, Physical layer measurements*" 3GPP TS 38.215 version 16.2.0 Release 16, July 2020.

[7] H.L. Bertoni: "*Radio propagation for modern wireless systems*", Prentice Hall, Upper Saddle River, 2000.

[8] M. Amorini: "*Studio della propagazione "Roof-to-Street" in sistemi cellulari operanti in ambiente urbano*", Master thesis in Telecommunications Engineering, University of Bologna, A.Y. 2001-2002.

[9] P. Bassi, C. Zaniboni: "Introduzione ai campi elettromagnetici", Bononia University Press, 2016.

[10] F. Fuschini, slides from lectures of "*Electromagnetic Propagation for Wireless Systems*" course.

[11] Georgia E. Athanasiadou, "*Fixed Wireless Access Propagation Modelling and Measurements*", 2009, IEEE

[12] Mauricio H. Dias, Glàucio L. Ramos, Glàucio L. Siqueira, "*Ray-Tracing Analysis of 3.5GHz Propagation at a Typical Urban Environment for FWA Systems*", 2001, IEEE

[13] M.P. Sellars, G.E. Athanasiadou, B. Ziolko, S.D. Greaves, A. Hopper, " *Simulation of Broadband FWA Networks in High-Rise Cities with Linear Antenna Polarisation*", 2003, IEEE.

[14] Elena-Madalina Oproiu, Iulian Gimiga, Ion Marghescu, "*5G Fixed Wireless Access – Mobile Operator Perspective*", 2018, IEEE.